Department of Physics and Astronomy
University of Heidelberg

Bachelor Thesis in Physics
submitted by

Tilman Hartwig

born in Karlsruhe (Germany)

2011

Determination of the Hubble Constant by Gravitational Lensing

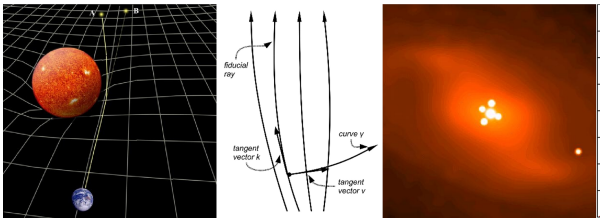

This Bachelor Thesis has been carried out by Tilman Hartwig at the
Institute of Theoretical Astrophysics in Heidelberg
under the supervision of
Prof. Dr. Matthias Bartelmann

Abstract

The Hubble constant is a fundamental parameter for describing the evolution and geometry of the universe. Using gravitationally lensed images of a source, we can determine the Hubble constant based on the time delay between individual images. In the framework of general relativity we derive the theory of gravitational lensing including light propagation on a curved manifold. We introduce the lensing potential, magnification and time delay and present various lens models. The mass-sheet degeneracy and several ways of breaking it are analysed. We review different approaches to determine the Hubble constant including a semianalytic CDM model proposed by Kochanek and a statistical assessment by Oguri. In order to obtain constraints for Hubble's parameter we study the error propagation and dependence on the mass model of a generalised lens system. Finally, we analyse the lens system B1608+656 regarding the model parameters' uncertainties. We present a list of quantities which should be determined more precisely in future and we obtain $H_0 = (48.3 \pm 26.7)$ km s^{-1}Mpc^{-1} assuming a lens model proposed by Myers et al.

Die Hubblekonstante ist ein grundlegender Parameter um die Form und Entwicklung des Universums zu beschreiben. Durch den Gravitationslinseneffekt sieht man mehrere Bilder einer Quelle und kann aus der Messung des Laufzeitunterschieds zwischen den Lichtwegen die Hubblekonstante bestimmen. Im Rahmen der Allgemeinen Relativitätstheorie leiten wir die Lichtausbreitung in einer gekrümmten Raumzeit ab und erhalten so die theoretischen Grundlagen des Gravitationslinseneffekts. Wir führen die Konzepte des Linsenpotentials, des Verstärkungseffekts und der Zeitverzögerung ein und stellen verschiedene Linsenmodelle vor. Die *mass-sheet degeneracy* wird untersucht und verschiedene Wege sie zu umgehen. Wir präsentieren mehrere Herangehensweisen zur Bestimmung der Hubblekonstanten mit dem Gravitationslinseneffekt wie z.B. ein semianalytisches CDM-Model von Kochanek oder einen statistischen Ansatz von Oguri. Die Fehlerfortpflanzung und die Abhängigkeit vom gewählten Massenmodell werden diskutiert, um so die Fehlergrenzen der Hubblekonstante abschätzen zu können. Wir untersuchen das Gravitationslinsensystem B1608+656 im Hinblick auf die Unsicherheiten der zu Grunde liegenden Messwerte und erhalten eine Auswahl an Parametern, die bei zukünftigen Messungen noch genauer bestimmt werden sollten, um den Fehler der Hubblekonstante klein zu halten. Wir erhalten schließlich einen Wert von $H_0 = (48.3 \pm 26.7)$ km s^{-1}Mpc^{-1}.

Contents

1 Introduction

The aim of this Bachelor Thesis is to explain the concepts of gravitational lensing and to present different methods of determining the Hubble constant based on time delays between multiple lensed images. Moreover we want to discuss the influence of errors and the mass model's dependency on Hubble's parameter.
The Hubble constant plays an important role in cosmology, it defines the universe's expansion, the critical densities and it is indispensable for general definitions of age and distance. We start with the history of Hubble's parameter and introduce Friedmann's expansion equations which describe fundamentally the evolution of the universe. The Hubble constant can be measured in many ways and we want to present the most common methods (Cepheids, Type Ia Supernovae, Sunyaev-Zeldovich Effect, CMB, Gravitational Lensing) and compare their advantages, disadvantages and precision.
In the next chapter we give a short outline of gravitational lensing's history and describe light propagation on a curved manifold. The Jacobi equation enables us to formulate the theory in a very general way and we obtain expressions for the lens equation, the lensing potential and the convergence. Thereafter we discuss the lens geometry, magnification, mass-sheet degeneracy and derive an expression for the time delay. A selection of lens models is presented at the end of this chapter.
There are various approaches to determine Hubble's parameter by gravitational lensing. We present the method of Kochanek who applies a semianalytic CDM model and points out that the Hubble constant solely depends on a few parameters. Additionally we discuss Oguri's statistical assessment of lens model dependences obtaining the relative strength of several perturbing components and a characterisation of stable image configurations.
In the last chapter we analyse the error propagation and dependence on the mass model. Therefore we derive an expression for the Hubble constant based on 13 parameters and study their individual influences. A singular isothermal ellipsoid with external shear represents the reference model and we adopt several simplifications and analyse the errors by assuming an inappropriate mass model. We apply this investigation to the lens system B1608+656 and obtain a list of parameters which should be measured more precisely in order to obtain proper values and reliable errors for Hubble's parameter. Finally we calculate a value for the Hubble constant based on a mass model proposed by Myers et al.

Acknowledgement:

I would like to thank Prof. Dr. Matthias Bartelmann for the interesting subject and the supervision of this work. I especially thank him for his encouragement, his accurate comments and his permanent support. Moreover I appreciate the interesting discussions with Vanessa Böhm and Sebastian Lorek who supported my work with creative ideas and useful hints. Special thanks go to Clio Bertelli Motta and Judith Hartwig for cross-reading my thesis and all those who contributed to the success of this work.

2 Hubble's Parameter

2.1 History

All time in history, people were thinking about the origin, the age and the size of the universe. Plato (428-348 B.C.) thought that the universe "is always in the same state" and "its maker [...] fashioned it complete and free from age and sickness" [1]. During the next 2000 years the idea of a static universe was established and even Einstein initially believed it to be static. Therefore he introduced the cosmological constant in his field equation in order to allow static solutions [2]. In the early 20th century Slipher discovered that most galaxies are moving away from us with very high velocities. In the 1920th Edwin Hubble analysed the escape velocities of distant galaxies and made a fundamental discovery: The further galaxies are away, the higher their escape velocities are. Hubble plotted the radial velocities against their distance and fitted a straight line in this observed data (figure 1). Actually he was convinced that there should be a linear relation due to Friedmann's equations and hence he had chosen the linear fit which turned out to be right. The

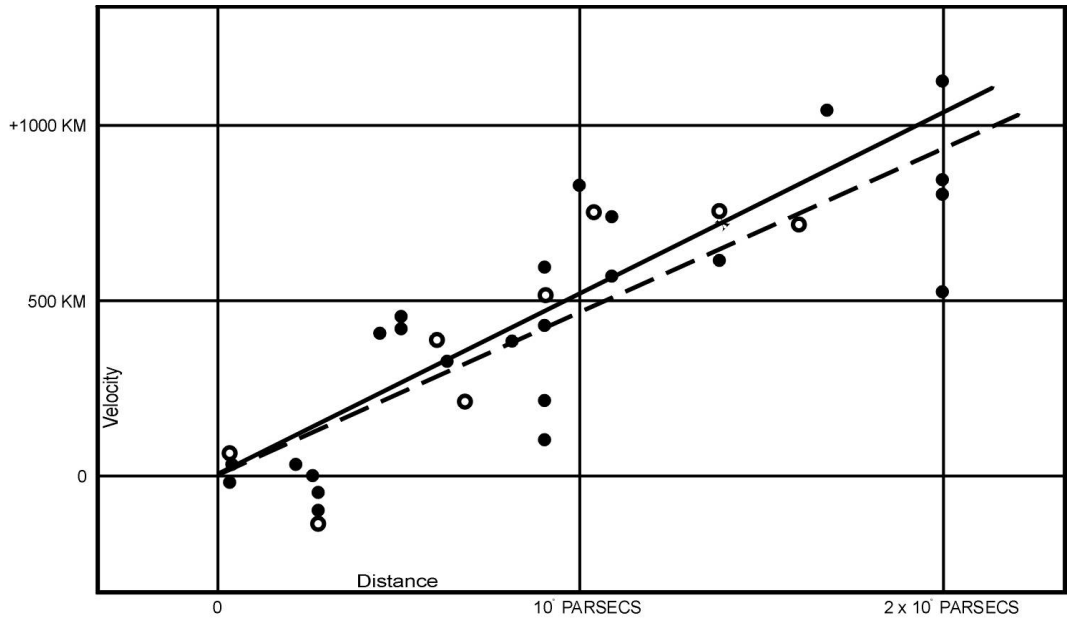

Figure 1: Radial velocities, corrected for solar motion, are plotted against distances estimated from involved stars and mean luminosities of nebulae in a cluster [3].

escape velocity v causes a Doppler shift of the galaxy's spectrum which can be observed as the redshift z. The linear relation then reads

$$v(r) = c\frac{\Delta\lambda}{\lambda} = cz = H_0 r \tag{2.1}$$

where H_0 is the proportionality constant which was subsequently named after Hubble. In 1929 Hubble published [3] a value of

$$H_0 = 530\frac{\text{km}}{\text{s Mpc}} \tag{2.2}$$

which is far too high compared to current measurements. But nevertheless Hubble provided the first hint that the universe is expanding and his linear relation turned out to be right at least for small redshifts. The determination of H_0 was very difficult because distant galaxies were hardly observable and nearby galaxies are gravitationally bound and can therefore not be considered in the global Hubble flow. The best measurement during the following years was by Sandage in 1958 [4] who proposed a value of

$$H_0 = 75\frac{\text{km}}{\text{s Mpc}} \tag{2.3}$$

which is very close to the current value published by Komatsu et al. in 2008 [5]

$$H_0 = (70.5 \pm 1.3)\frac{\text{km}}{\text{s Mpc}}. \tag{2.4}$$

Frequently Hubble's parameter is expressed in a dimensionless way by defining

$$H_0 = 100h\frac{\text{km}}{\text{s Mpc}}. \tag{2.5}$$

The unit of the Hubble Constant is chosen according to the relation between escape velocity and distance but actually it has the unit of an inverse time. Hence we can define the Hubble time

$$\tau_0 = \frac{1}{H_0} \approx 13.9 \cdot 10^9 \text{a} \tag{2.6}$$

which represents the age of the universe in a uniformly expanding model. In the same way one can define the Hubble radius or Hubble length

$$R_H = \frac{c}{H_0} \approx 4255\text{Mpc}. \tag{2.7}$$

It is a typical length scale for all distances in an expanding universe. Without knowing much about cosmology we can already see that the Hubble constant is a fundamental parameter for describing the evolution and geometry of the universe. To obtain more precise equations and results we have to derive Friedmann's Expansion Equations.

2.2 Friedmann's Expansion Equations

2.2.1 Expansion Rate

The cosmological principle states that the universe is homogeneous and isotropic on sufficiently large scales. Obviously the cosmological principle has to be wrong on small scales because otherwise humanity might not be able to formulate it. We introduce a spherical coordinate system which is allowed to expand with time and consider a sphere with homogeneous density and a particle at the location $\vec{x}$. Due to the cosmological principle the expansion and the time dependent position $\vec{r}(t)$ can be expressed by

$$\vec{r}(t) = a(t)\vec{x} \tag{2.8}$$

with the cosmic scale factor $a(t)$ which does only depend on time. Per convention the scale factor is set to $a(t_0) = 1$ for $t_0 =$ today. Because of isotropy we can use scalar quantities r and x instead of $\vec{r}$ and $\vec{x}$. For the velocity of our test particle caused by the cosmic expansion we derive

$$v(r,t) = \frac{\mathrm{d}}{\mathrm{d}t}r(t) = \frac{\mathrm{d}a(t)}{\mathrm{d}t}x = \dot{a}(t)x = \frac{\dot{a}(t)}{a(t)}r = H(t)r \tag{2.9}$$

where we used equation 2.1 in the last step. As we will see later on $\ddot{a} \neq 0$ which leads to a time dependent Hubble constant and $H_0 = H(t_0)$ only represents the current local expansion. Equation 2.9 is a generalisation of the time independent Hubble law and we can define an expansion rate

$$H(t) = \frac{\dot{a}}{a}. \tag{2.10}$$

2.2.2 Dynamics of the Expansion

We are interested in the evolution of the scale factor $a(t)$ because it describes the development of our universe. To derive the Friedmann Equations in the most general form, we have to start from

Einstein's field equation

$$G_{\mu\nu} = \frac{8\pi G}{c^4} T_{\mu\nu} + \Lambda g_{\mu\nu}. \tag{2.11}$$

The energy-momentum tensor $T^{\mu\nu}$ includes all kinds of energy and acts as the source of gravity. Generally it has the components $T^{\mu\nu} = (\rho c^2 + p)u^\mu u^\nu + p g^{\mu\nu}$ for a perfect fluid but in our case it has to be diagonal and the components must not depend on spatial coordinates in order to preserve homogeneity and isotropy. Therefore we can set

$$T_{00} = \rho c^2, \qquad T_{ij} = p\delta_{ij}. \tag{2.12}$$

$G^{\mu\nu}$ is the Einstein tensor which depends on the structure of space time and Λ is the cosmological constant. The field equation is a system of 10 non-linear 2^{nd} order partial differential equations and describes how energy and geometry influence each other. The Robertson-Walker metric

$$g = -c^2 \mathrm{d}t^2 + \left(\frac{a(t)}{1 + \frac{kr^2}{4}} \right)^2 \left(\mathrm{d}x^2 + \mathrm{d}y^2 + \mathrm{d}z^2 \right) \tag{2.13}$$

is a general form of a spatially homogeneous and isotropic metric. We can introduce an appropriate dual basis

$$\theta^0 = c\mathrm{d}t, \qquad \theta^i = \frac{a(t)\mathrm{d}x^i}{1 + \frac{kr^2}{4}} \tag{2.14}$$

and use Cartan's structure equations to derive expressions for the Ricci tensor and the Ricci scalar. Hence the Einstein tensor has the components

$$G_{00} = 3\frac{k + \left(\frac{\dot{a}}{c}\right)^2}{a^2}, \qquad G_{11} = G_{22} = G_{33} = -\frac{2\ddot{a}}{c^2 a} - \frac{k + \left(\frac{\dot{a}}{c}\right)^2}{a^2}. \tag{2.15}$$

Assuming an ideal fluid, the field equation transforms into

$$H(t)^2 = \left(\frac{\dot{a}}{a} \right)^2 = \frac{8\pi G}{3}\rho + \frac{\Lambda}{3} - \frac{kc^2}{a^2} \tag{2.16}$$

and

$$\frac{\ddot{a}}{a} = -\frac{4\pi G}{3}\left(\rho + \frac{3p}{c^2} \right) + \frac{\Lambda}{3} \tag{2.17}$$

which is known as Friedmann's equations. We split up the density ρ into non relativistic matter $\rho_m(t) = \rho_{m0} a(t)^{-3}$ and relativistic matter $\rho_r(t) = \rho_{r0} a(t)^{-4}$ which scales as a^{-4} because it is additionally redshifted by the cosmic expansion. Furthermore we can define the constant vacuum energy density $\rho_v = \Lambda / 8\pi G$ and the critical density $\rho_{cr} = 3H_0^2 / 8\pi G$. It is convenient to introduce dimensionless density parameters for matter, radiation and vacuum energy

$$\Omega_m = \frac{\rho_m}{\rho_{cr}}, \qquad \Omega_r = \frac{\rho_r}{\rho_{cr}}, \qquad \Omega_\Lambda = \frac{\rho_v}{\rho_{cr}} = \frac{\Lambda}{3H_0^2} \tag{2.18}$$

and we notice that Ω_m and Ω_r depend on time whereas Ω_Λ is time independent. Introducing the curvature parameter

$$\Omega_k = -\frac{kc^2}{H_0^2} = 1 - \Omega_m - \Omega_r - \Omega_\Lambda \tag{2.19}$$

and subtracting the first from the second Friedmann equation yields

$$\left(\frac{\dot{a}(t)}{a(t)} \right)^2 = {H_0}^2 \left[a(t)^{-4}\Omega_r + a(t)^{-3}\Omega_m + a(t)^{-2}\Omega_k + \Omega_\Lambda \right]. \tag{2.20}$$

This fundamental equation contains all information about geometry, matter and energy in the universe and completely describes its expansion.

2.2.3 Measurement of Time and Distance

Due to a curved space time and an expanding universe we have to clarify quantities like age and distance in our metric. Using the relation

$$\mathrm{d}t = \frac{\mathrm{d}a}{\dot{a}} = \frac{\mathrm{d}a}{aH(a)} \tag{2.21}$$

one can calculate the age of the universe depending on the scale factor

$$t(a) = \frac{1}{H_0}\int_0^a \mathrm{d}a \left[a^{-2}\Omega_r + a^{-1}\Omega_m + \Omega_k + a^2\Omega_\Lambda\right]^{-1/2}. \tag{2.22}$$

Together with

$$1 + z = \frac{1}{a} \tag{2.23}$$

we have direct relations between the physical age t, the redshift z and the scale factor a. In the same way we can use the relation $-c\mathrm{d}t = a\mathrm{d}w$ for photons to express the distance of a source based on its redshift. The comoving radial distance can be integrated to obtain

$$\int \mathrm{d}w = -\int_{a=1}^{a_{\mathrm{src}}} \frac{c\mathrm{d}t}{a} \tag{2.24}$$

where a_{src} denotes the scale factor depending on the redshift of the source. Using again the relation $\mathrm{d}t = \mathrm{d}a/aH$ and the Friedmann equation we can write

$$w = -\int_{a=1}^{a_{\mathrm{src}}} \frac{\mathrm{d}a}{a}\frac{c}{H_0}\left[a(t)^{-4}\Omega_r + a(t)^{-3}\Omega_m + a(t)^{-2}\Omega_k + \Omega_\Lambda\right]^{-1/2}. \tag{2.25}$$

Unfortunately analytical solutions for equation 2.22 and 2.25 are only available for special cases and we have to use numerical methods or simplify matters by assuming different cosmological cases. The qualitative behaviour of $a(t)$ can be seen in Figure 2. Regarding the analytical solution of equation 2.20 we notice that every density parameter contributes with a different power of a and therefore we can conclude that in the early universe Ω_r was dominating (radiation dominated epoch), followed by a matter dominated epoch and nowadays Ω_Λ is the most dominant term. As we want to deal with gravitational lensing, we can neglect Ω_r and focus on the matter dominated epoch. In the Einstein-de-Sitter-universe we set $\Omega_m = 1$ which describes the expansion sufficiently well. For the Einstein-de-Sitter-universe equation 2.22 has the simple solution

$$a(t) = \left(\frac{3H_0 t}{2}\right)^{2/3} \tag{2.26}$$

and the comoving radial distance in an Einstein-de-Sitter-universe can be expressed by

$$w(z) = \frac{2c}{3H_0}\left(1 - \frac{1}{(1+z)^{3/2}}\right). \tag{2.27}$$

We see that the Hubble constant plays an important role in cosmology. It defines the universe's expansion, the critical densities and it is fundamental for the translation between time, scale factor, redshift and comoving distances. Therefore it is important to measure H_0 with high accuracy and in the next section we want to discuss different methods.

2.3 Measuring the Hubble Constant

There are various methods for measuring Hubble's parameter, based on different astrophysical effects. In this section we want to discuss the most common ones and we are particularly interested in the precision of each method. Therefore we analyse and compare the errors and plot the

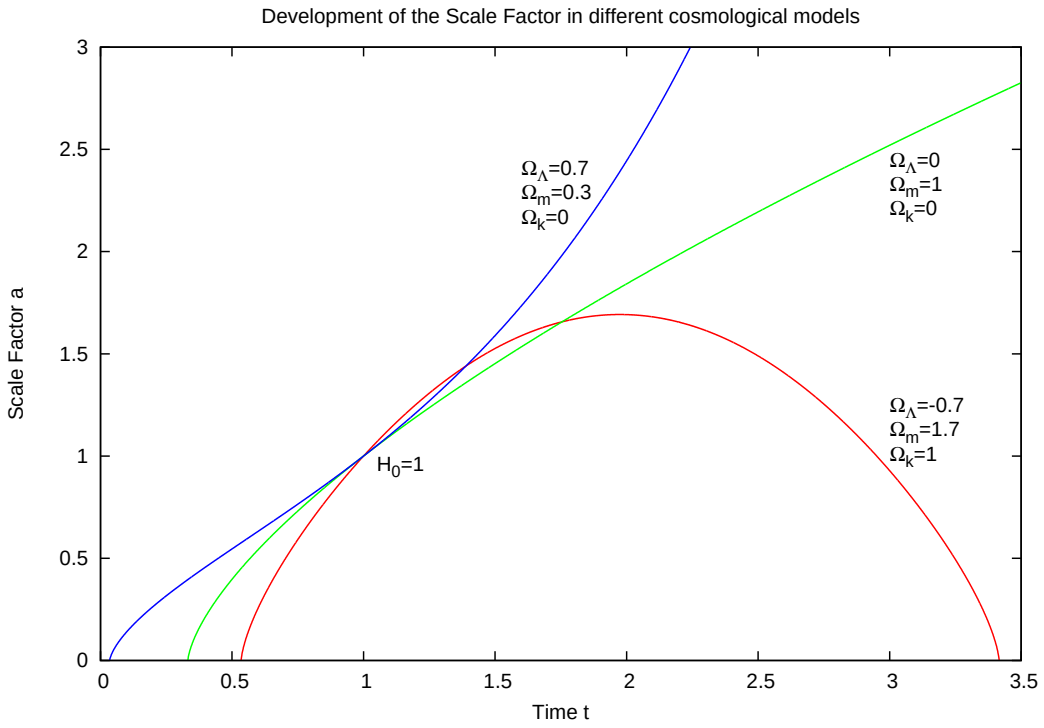

Figure 2: Numerical solutions for equation 2.20 ($\Omega_r \approx 0$) integrated with a one step Euler scheme. $H_0 = 1$ is the measurable boundary value and represents the gradient for all solutions at $t = 1$. The red curve describes a closed universe which will collapse in future. The green solution is an Einstein-de-Sitter-universe and the blue one describes an accelerated expansion. All curves have in common, that they reach $a = 0$ for small t which can be seen as a proof for the big bang.

development of the measurement's accuracy. The data for this analysis is provided by John Huchra [6] who attempts to collect all measurements of the Hubble constant. The relative error for each method is the median of the relative errors listed by Huchra.

2.3.1 Local Hubble Law

The linear relation $v = H_0 r$ is only valid for objects in the local Hubble flow. That means that they should be far enough away to be considered gravitationally unbound but still close enough so that nonlinear cosmological effects are negligible. If we observe sources in this regime, we can measure their escape velocity and their distance in order to calculate H_0. The escape velocity v can easily be calculated by the redshift z which can be measured with high precision by spectroscopy (figure 3). The relation $v = cz$ is only valid for non relativistic velocities and yields the escape

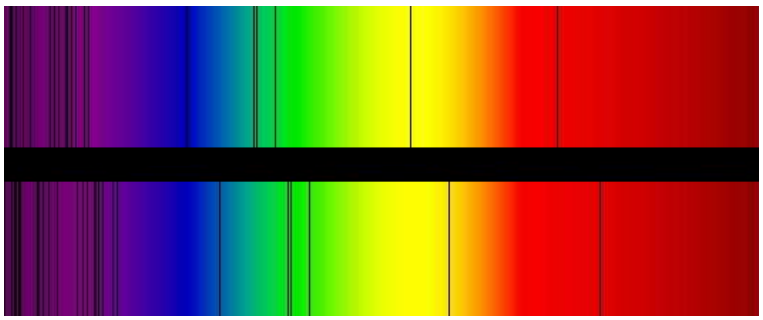

Figure 3: Absorption lines in the optical spectrum of the supercluster BAS11 (top) compared to those in the optical spectrum of the Sun (bottom) [7].

velocity. The distance r of an object is more difficult to measure and there are several methods. Therefore we just want to discuss the most popular ones for measuring r and determining the

Hubble constant.

Cepheids Cepheids are variable stars with a well-defined relation between their period and luminosity. First one has to calibrate the period-luminosity-relation using Cepheids in our own galaxy or nearby galaxies. We can determine their apparent magnitude by observation, measure the distance by parallax and calculate their absolute magnitude in order to relate it to the period. Unfortunately, most suitable cepheids are more than 250pc away and the distance measurement has a systematic error of about 10% [8]. Nevertheless, after calibrating the Cepheids, they are suitable as standard candles: By knowing the period of a variable star we can determine its absolute magnitude and therefore the distance with the help of the distance-modulus. This method was one of the first extragalactic distance measurements but the period luminosity relation depends on the metallicity which is a further uncertainty. Additionally we have to keep in mind, that it is based on the so called distance ladder which describes the fact that astronomical distance measurements depend on each other: The fundamental length scale in the solar system is the astronomic unit (au) which can nowadays be measured with high precision. Based on the au we can define one parsec which is a suitable length scale for the Milky Way and nearby galaxies. Based on the definition of one parsec we can introduce standard candles or even more sophisticated distance measurements. Summing up, the distance ladder is effected by error propagation from step to step which leads to uncertainties especially on large scales. Nowadays, Cepheids are no longer applicable for direct distance measurements but they are helpful to define further standard candles.

Type Ia Supernovae (SNe Ia) SNe Ia are very luminous explosions of white dwarfs with a characteristic light curve and a typical peak brightness. Due to the luminosity and their well-defined absolute magnitudes and light curve shape, SNe Ia are very common as standard candles on cosmological scales. Therefore we have to find sufficient SNe Ia at known distances to gauge the distance latter but at the moment this number is limited to six objects [9] which leads to significant statistical uncertainties. Based on this calibration, the apparent peak brightness can be measured and related to their distance with an intrinsic scatter of $< 10\%$ [8]. The relative error of the Hubble constant with this method is $\Delta H_0/H_0 \approx 8\%$ and the development of the measurements is shown in figure 4.

Sunyaev–Zeldovich Effect In principle, the cosmic microwave background (CMB) has a well-defined black body distribution but a lot of effects cause systematic deviations from this slope. Passing through hot gas of rich clusters of galaxies or any other plasma, the CMB-photons experience an inverse-Compton scattering. The Sunyaev–Zeldovich effect was investigated in 1970 and describes this redistribution of CMB-photons which are more energetic after scattering. We can now use the fact, that the measured X-ray flux from the plasma depends on the distance, but the caused energy shift of some CMB-photons is distance independent and valid for all redshifts. This relation leads to a distance measurement and can therefore be used to calculate the Hubble constant. The main uncertainties of this method result from potential substructure in the gas of the cluster, projection effects, the assumption of hydrostatic equilibrium and details of the models for the gas and electron densities [8]. Due to these systematics, the Hubble constant can only be estimated up to an accuracy of about $\Delta H_0/H_0 \approx 19\%$ with the Sunyaev–Zeldovich effect. The development of the measurements is shown in figure 5.

2.3.2 CMB

CMB observations do not directly measure the local expansion rate of the universe rather they measure the conformal distance to the decoupling surface and the matter-radiation ratio through the amplitude of the early integrated Sachs-Wolfe contribution relative to the height of the first peak [10]. The power spectrum describes the angular correlation of the CMB fluctuations and it

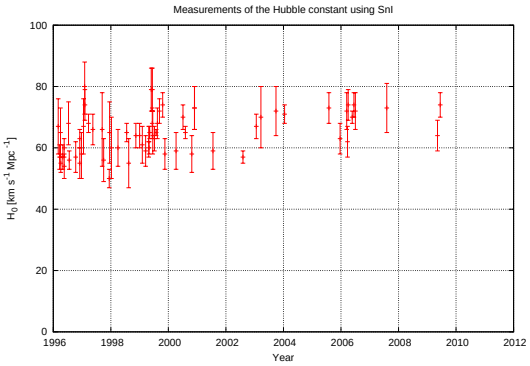

Figure 4: Measurement of H_0 using Type Ia Supernovae.

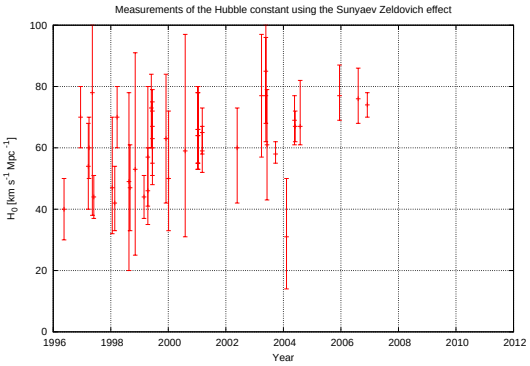

Figure 5: Measurement of H_0 using the Sunyaev–Zeldovich effect.

can be fitted via H_0 and other cosmological parameters. This correlation between parameters is a source of systematic errors: As long as we can not fix the other cosmological parameters (Ω_Λ, Ω_m, w, σ_8) properly, we are left with a uncertainty regarding the Hubble constant. Komatsu et al. were able to determine H_0 with an accuracy of 4% with this method [11] where he included further cosmological data. Generally, the relative error of this method is $\Delta H_0/H_0 \approx 9\%$ and the development of the measurements is shown in figure 6.

2.3.3 Gravitational Lensing

Another approach to measure the Hubble constant is based on the time delay between different images of a gravitationally lensed source. The total time delay is proportional to the inverse Hubble constant. By understanding the effect, systematics can be turned into statistical errors and H_0 can be measured very precisely. The Hubble constant's relative error is $\Delta H_0/H_0 \approx 13\%$ with this method and the development of the measurements is shown in figure 7. Although the relative error is higher compared to other methods, we have to emphasise that gravitational lensing does not depend on distance ladders and is very insensitive to changes of the cosmological model. Therefore this methods provides an independent way of measuring Hubble's parameter. Suyu et al. obtain a value of $H_0 = (70.6 \pm 3.1)\text{km s}^{-1}\text{Mpc}^{-1}$ [12].

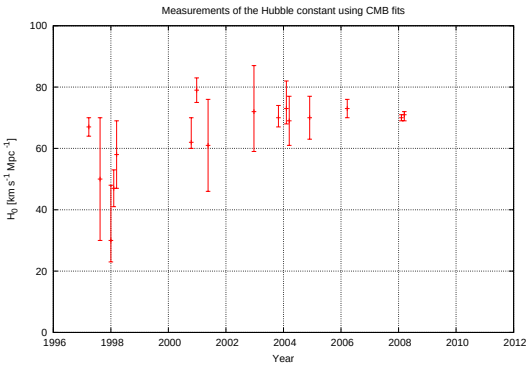

Figure 6: Measurement of H_0 using a fit to the CMB.

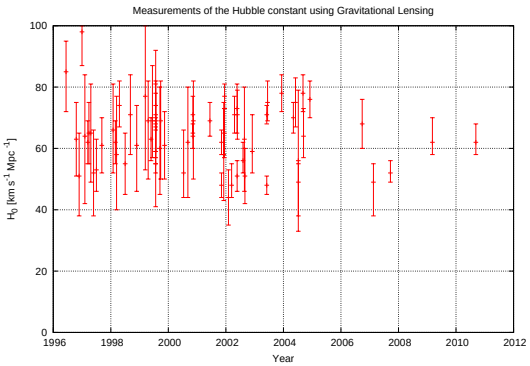

Figure 7: Measurement of H_0 using gravitational lensing.

3 Gravitational Lensing

Gravitational Lensing is based on light deflection in a curved space-time and can be used to study the mass distribution of galaxies or clusters and to derive cosmological parameters. We want to understand the historical background regarding lensing theory and experimental proofs. Then we derive a general formalism for light propagation on a curved manifold based on the Jacobi equation. This formalism enables us to analyse various gravitational lensing effects like magnification, convergence, shear and time delay. Furthermore we want to study the dependence of the time-delay on cosmological parameters which leads to the determination of the Hubble constant by gravitational lensing. To apply this theory we have to find suitable lens models which will also be presented in this chapter.
The following theoretical deviation of light propagation and gravitational lensing is mainly based on a review article by M. Bartelmann [13], the book "Extragalactic Astronomy and Cosmology" by P. Schneider [14], lecture notes "Lectures on Gravitational Lensing" by R. Narayan and M. Bartelmann [15], the book "Gravitational Lensing: Strong, Weak and Micro" by P. Schneider, C. Kochanek and J. Wambsganss [16] and the script "General Relativity" by M. Bartelmann [17].

3.1 History

The theory of gravitational lensing is based on the general theory of relativity published by Einstein in 1915. He replaced Newton's theory of gravity by a more general formalism which states, that space time can be seen as a manifold and its curvature is defined by its matter and energy content. A first experimental proof of this theory was the perihelion precession of mercury which was previously believed to be measurement errors or external perturbations. But a second proof was given by Sir A. S. Eddington in 1919: Light moves along geodesics in this space time and is therefore deflected by mass distributions. A light ray passing from a star behind the sun close to its surface should be deflected and we should be able to observe it although it is located behind the sun (Figure 8). Obviously this effect is only observable during solar eclipses. In May 1919 Eddington

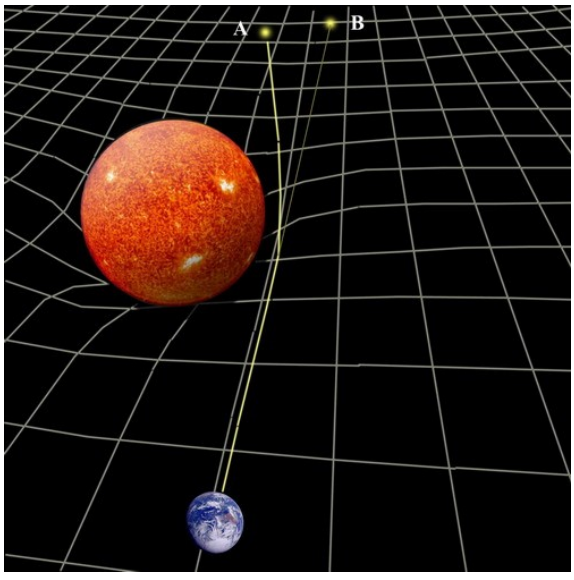

Figure 8: Light deflection of a ray passing close to the sun's surface. The actual position A is behind the sun and not observable but due to bending of the light ray we observe the star at the apparent position B [18].

observed a solar eclipse in West Africa and was able to measure the light deflection. Figure 9 shows one of Eddington's photos which illustrates the deflected positions. He published his results in 1920 and states that "the course of a ray of light is in accordance with Einstein's generalised relativity theory. This leads to an apparent displacement of a star at the limb amounting to $1''75$

outwards" [19]. This discovery was not only a remarkable evidence of Einstein's theory but also

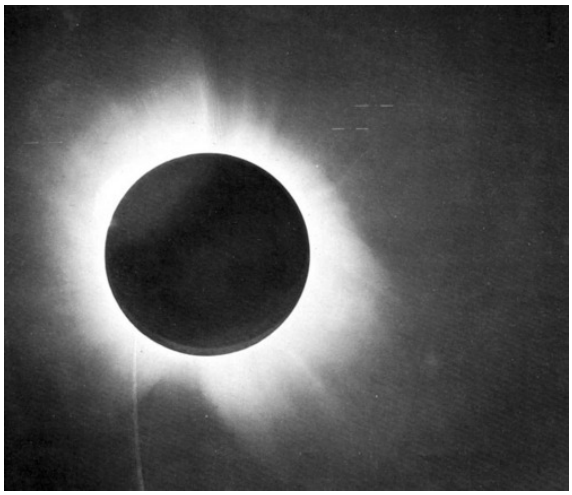

Figure 9: Eddington's photo of a total eclipse taken on May 29, 1919 in West Africa. Deflected stars are shown between white marks in the top right of the sun [19].

the basis for gravitational lensing. In 1924 Chwolson wrote an article about the possibility to see two images from one star whose light rays are deflected by another massive star [20]. This was the first hint for gravitational lensing although Chwolson himself was not sure whether this effect really exists.
It was again Einstein who contributed to the theoretical background in 1936 [21]. He was the first who spoke about a "lens like action" referring to the increase of the apparent brightness by this effect and he introduced the concept of Einstein rings which were subsequently named after him. Einstein thought that "there is no great chance of observing this phenomenon" but nevertheless scientists have tried to find experimental evidence for gravitational lenses. Up to the 1930s it was assumed,

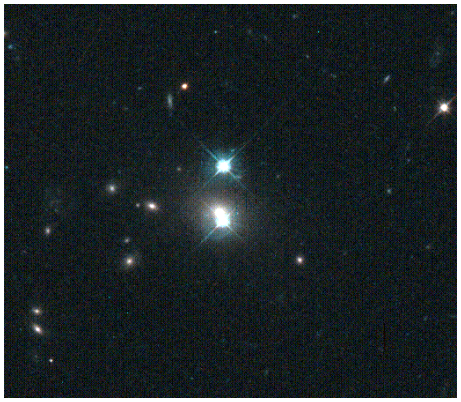

Figure 10: First observation of a gravitational lens. The two bright blue sources are the quasar Q0957+561 lensed by the giant elliptical galaxy Q0957+561 G1 [22].

that only stars in our own galaxy could act as gravitational lenses. But in 1937 F. Zwicky expanded this belief and considered lensing by "extragalactic nebulae" which we nowadays know as galaxies. Using his mass estimation for the galaxy, he calculated the typical image separation of a background source to be of the order $10''$, which was already observable with telescopes. Additionally, Zwicky pointed out that distant galaxies would be magnified and therefore might be detectable even if their unlensed luminosity is below the observational threshold. The theory of gravitational lensing outside our own galaxy improved during the following years and the historically most important article for this thesis was published in 1964 by Sjur Refsdal [23]. He pointed out that the time delay between different lensed images of one source can be used to determine the Hubble constant. The value of H_0 might only depend on the time delay Δt, the redshifts of source and lens, the luminosity

of the images and the angle between them. Based on assumptions regarding the absolute magnitude of supernovae, galaxy masses, mean angular separations and redshifts he concluded that "a double image of a supernova within a distance $6 \cdot 10^8$pc should be possible to observe every third year". Actually, the first gravitational lens was discovered in 1979 by Dennis Walsh, Bob Carswell, and Ray Weymann. They discovered it accidentally and named it "Twin QSO" because it initially looked like two similar quasistellar objects (figure 10). In the following years, the number of observed gravitational lenses increased as observation methods became more precise and computers enable simultaneous measurements of million of sources. A very popular and impressive gravitational lens is the Einstein Cross Q2237+030 figure 11). It is a gravitationally lensed quasar that is located

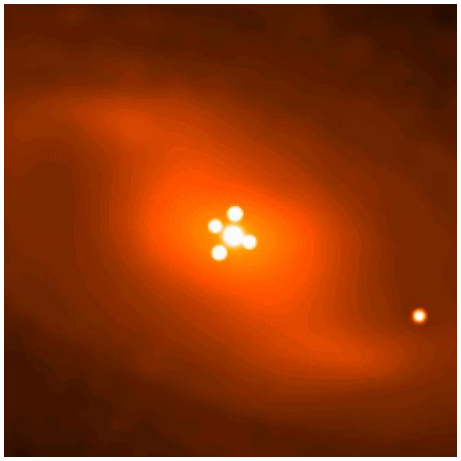

Figure 11: Einstein Cross. The apparent dimension of this galaxy is 0.87×0.34 arcminutes, while the apparent dimension of the cross in its centre accounts for only 1.6×1.6 arcseconds [24].

directly behind ZW2237+030. This constellation produces four images of the same quasar with almost equal brightness.

3.2 Light Propagation on a Curved Manifold

To understand the theory of gravitational lensing, we have to study the effects of light deflection on a curved manifold. Generally we assume that the universe can be described by a Friedmann-Lemaître-Robertson-Walker-metric and that the cosmological principle is valid on sufficiently large scales. Nevertheless, we need matter inhomogeneities on small scales to produce lensing effects but we require these inhomogeneities to have small Newtonian gravitational potentials, namely $\Phi \ll c^2$. Furthermore we assume that the peculiar velocities of the gravitational lenses are small ($v \ll c$) and their motion is dominated by the mean cosmic flow. These assumptions are sufficiently valid for all effects discussed within this thesis.

3.2.1 Jacobi Equation

Light propagation in arbitrary space times can be described by the Jacobi equation and therefore we want to motivate this important equation.
We assume a congruence of null geodesics which should represent a bundle of light rays (figure 12). The geodesic curve is parametrised by the so far arbitrary parameter λ and its tangent vector can be written as $\tilde{k} = \partial_\lambda$ with the normalisation $\langle \tilde{k}, \tilde{k} \rangle = 0$. By definition, this tangent vector is parallel transported along the geodesic

$$\nabla_{\tilde{k}} \tilde{k} = 0. \tag{3.1}$$

We introduce a second curve γ which is transversal to the congruence and is parametrized by the parameter σ. The curve γ connects the fiducial light ray with a neighbouring ray and its tangent

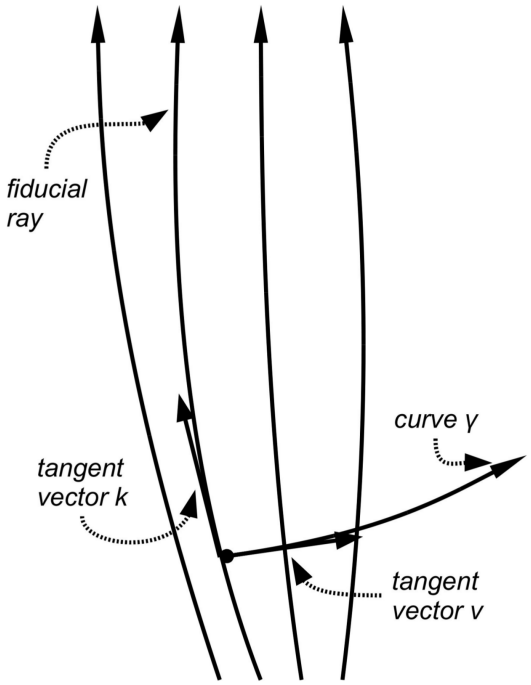

Figure 12: A congruence of null geodesics with the fiducial light ray and its tangent vector k. The curve γ connects rays in the bundle and has the tangent vector v [13].

vector can be expressed as

$$v = \dot{\gamma} = \partial_\sigma. \tag{3.2}$$

Since the partial derivatives with respect to the curve parameters λ and σ commute, so do the vectors $\tilde{k}$ and v and we can conclude that v is Lie-invariant along $\tilde{k}$

$$0 = [\tilde{k}, v] = \mathcal{L}_{\tilde{k}} v. \tag{3.3}$$

Next, we introduce a vector

$$n = v + \langle v, \tilde{k}\rangle \tilde{k} \tag{3.4}$$

which is perpendicular to $\tilde{k}$

$$\langle n, \tilde{k}\rangle = 0. \tag{3.5}$$

The Lie-derivative of n along $\tilde{k}$ yields

$$\mathcal{L}_{\tilde{k}} n = [\tilde{k}, n] = [\tilde{k}, v] + [\tilde{k}, \langle v, \tilde{k}\rangle \tilde{k}] = \tilde{k}\langle v, \tilde{k}\rangle \tilde{k} = (\partial_\lambda \langle v, \tilde{k}\rangle)\tilde{k} \tag{3.6}$$

where we used equation 3.3. Since $\langle \tilde{k}, \tilde{k}\rangle = 0$ we can write

$$0 = \partial_\lambda \langle \tilde{k}, \tilde{k}\rangle = v\langle \tilde{k}, \tilde{k}\rangle = 2\langle \nabla_v \tilde{k}, \tilde{k}\rangle \tag{3.7}$$

using the Jacobi identity $[x,[y,z]] + [z,[x,y]] + [y,[z,x]] = 0$. The connection is symmetrical and the commutator between $\tilde{k}$ and v vanishes which implies $\nabla_v \tilde{k} = \nabla_{\tilde{k}} v$ from where we can derive

$$\partial_\lambda \langle \tilde{k}, v\rangle = \tilde{k}\langle \tilde{k}, v\rangle = \langle \nabla_{\tilde{k}} \tilde{k}, v\rangle + \langle \tilde{k}, \nabla_{\tilde{k}} v\rangle = \langle \tilde{k}, \nabla_v \tilde{k}\rangle. \tag{3.8}$$

Together with equation 3.6 we can conclude that n is Lie-transported along the light ray

$$\mathcal{L}_{\tilde{k}} n = 0. \tag{3.9}$$

As n denotes the perpendicular separation vector between neighbouring geodesics it is Lie-invariant along the congruence. Using the fact that $\tilde{k}$ and v commute and that $\tilde{k}$ is a geodesic, we can rewrite the second derivative of v along $\tilde{k}$

$$\nabla^2_{\tilde{k}} v = \nabla_{\tilde{k}} \nabla_{\tilde{k}} v = \nabla_{\tilde{k}} \nabla_v \tilde{k} = (\nabla_{\tilde{k}} \nabla_v - \nabla_v \nabla_{\tilde{k}}) \tilde{k} \tag{3.10}$$

and see that it is equivalent to the curvature applied to $\tilde{k}$ and v

$$R(\tilde{k}, v)\tilde{k} = (\nabla_{\tilde{k}} \nabla_v - \nabla_v \nabla_{\tilde{k}}) \tilde{k}. \tag{3.11}$$

This is expressed by the Jacobi equation

$$\nabla^2_{\tilde{k}} v = R(\tilde{k}, v)\tilde{k} \tag{3.12}$$

which describes how the vector v changes along the ray in response to the curvature. In a next step we want to find a similar equation for the separation vector n. First we can calculate that

$$\nabla_{\tilde{k}} n = \nabla_{\tilde{k}} v + \nabla_{\tilde{k}} (\langle v, \tilde{k} \rangle \tilde{k}) = \nabla_{\tilde{k}} v + (\partial_\lambda \langle v, \tilde{k} \rangle) \tilde{k} = \nabla_{\tilde{k}} v \tag{3.13}$$

and use this result to derive

$$\nabla^2_{\tilde{k}} n = \nabla^2_{\tilde{k}} v. \tag{3.14}$$

Furthermore we use the linearity of the curvature

$$R(\tilde{k}, n) = R(\tilde{k}, v + \langle \tilde{k}, v \rangle \tilde{k}) = R(\tilde{k}, v) + \langle \tilde{k}, v \rangle R(\tilde{k}, \tilde{k}) = R(\tilde{k}, v) \tag{3.15}$$

to derive another form of the Jacobi equation which is often called the equation of geodesic deviation

$$\nabla^2_{\tilde{k}} n = R(\tilde{k}, n)\tilde{k}. \tag{3.16}$$

It describes directly how the separation between neighbouring geodesics evolves along the ray according to curvature.

3.2.2 Propagation of a Light Bundle

We want to use the Jacobi equation to study the behaviour of an arbitrary light ray on a curved manifold. Therefore we introduce a screen which is perpendicular to the tangent vector $\tilde{k}$. This screen is also perpendicular to the propagation direction of the light ray and is spanned by the vectors $E_{1,2}$ which are parallel transported along the ray

$$\nabla_{\tilde{k}} E_i = 0 \tag{3.17}$$

and can be combined to a complex vector $\epsilon = E_1 + iE_2$. Equation 3.12 can be written as a matrix equation

$$\nabla^2_{\tilde{k}} \begin{pmatrix} v^1 \\ v^2 \end{pmatrix} = \mathcal{T} \begin{pmatrix} v^1 \\ v^2 \end{pmatrix} \tag{3.18}$$

with the so called tidal matrix

$$\mathcal{T} = \begin{pmatrix} \mathcal{R} + \Re(\mathcal{F}) & \Im(\mathcal{F}) \\ \Im(\mathcal{F}) & \mathcal{R} - \Re(\mathcal{F}) \end{pmatrix} \tag{3.19}$$

and its components

$$\mathcal{R} = -\frac{1}{2}R_{\alpha\beta}\tilde{k}^{\alpha}\tilde{k}^{\beta} + \frac{1}{2}C_{\alpha\beta\gamma\delta}\epsilon^{\alpha}\tilde{k}^{\beta}\tilde{k}^{\gamma}\epsilon^{*\delta}, \tag{3.20}$$

$$\mathcal{F} = \frac{1}{2}C_{\alpha\beta\gamma\delta}\epsilon^{\alpha}\tilde{k}^{\beta}\tilde{k}^{\gamma}\epsilon^{\delta}. \tag{3.21}$$

The Weyl curvature $C_{\alpha\beta\gamma\delta}$ will be discussed and specified below. We are allowed to distinguish between different curvature contributions: On the one hand we have the background curvature in the homogeneous and isotropic universe described be the Friedmann-Lemaître-Robertson-Walker metric and on the other hand we have local matter contributions and structure inhomogeneities described by their gravitational potential. This division is verified by our assumptions of small peculiar velocities and weak gravitational fields of the inhomogeneities. Therefore we are allowed to split up the tidal matrix into a background part and clump contributions:

$$\mathcal{T} = \mathcal{T}_{\mathrm{bg}} + \mathcal{T}_{\mathrm{cl}}. \tag{3.22}$$

3.2.3 Background Contribution

In order to describe the background contribution, we introduce the Friedmann-Lemaître-Robertson-Walker metric

$$\mathrm{d}s^2 = a(\eta)^2\left(-\mathrm{d}\eta^2 + \mathrm{d}w^2 + f_K^2(w)\mathrm{d}\Omega^2\right) \tag{3.23}$$

with the spatial curvature K and the conformal time η which is related to the coordinate time by $a\mathrm{d}\eta = c\mathrm{d}t$. The comoving angular-diameter distance f_K as a function of the comoving radial distance w can be expressed as:

$$f_K(w) = \begin{cases} \frac{1}{\sqrt{K}}\sin(\sqrt{K}w) & K > 0 \\ w & K = 0 \\ \frac{1}{\sqrt{-K}}\sinh(\sqrt{-K}w) & K < 0 \end{cases} \tag{3.24}$$

The Weyl curvature has to vanish for the homogeneous contribution because we assume the space time to be symmetric and locally flat, but we are still left with the contribution of the Ricci tensor $R_{\alpha\beta}$. Since $\tilde{k}$ is a null vector, we can directly relate the Ricci tensor to the energy-momentum tensor $T_{\alpha\beta}$ by Einstein's field equation

$$R_{\alpha\beta}\tilde{k}^{\alpha}\tilde{k}^{\beta} = G_{\alpha\beta}\tilde{k}^{\alpha}\tilde{k}^{\beta} = \frac{8\pi G}{c^4}T_{\alpha\beta}\tilde{k}^{\alpha}\tilde{k}^{\beta}. \tag{3.25}$$

Assuming the energy-momentum tensor of an ideal fluid with negligible pressure, we can write

$$T_{\alpha\beta}\tilde{k}^{\alpha}\tilde{k}^{\beta} = \rho c^2\langle u, \tilde{k}\rangle^2 \tag{3.26}$$

with the velocity u of a comoving observer. If we set $\tilde{k}\omega_{\mathrm{obs}} = k$, the projection gives the (negative) frequency ω_{obs} measured by an observer

$$|\langle\tilde{k}, u\rangle| = \frac{|\langle k, u\rangle|}{\omega_{\mathrm{obs}}} = \frac{\omega}{\omega_{\mathrm{obs}}} = 1 + z. \tag{3.27}$$

As we have seen before, matter density evolves as $\rho = \rho_0(1+z)^3$ with the density ρ_0 measured by the comoving observer. Now we can express the diagonal elements of the tidal matrix by

$$\mathcal{R} = -\frac{4\pi G}{c^2}\rho_0(1+z)^5. \tag{3.28}$$

In a next step we want to solve the Jacobi equation for this background contribution. According to our normalization of $\tilde{k}$ we have to choose λ such that $|\langle\tilde{k}, u\rangle| = 1 + z$. Based on our assumption that peculiar velocities are negligible we can project $\tilde{k}$ on the mean flow velocity $u^\mu = \delta^\mu_0$ and have to satisfy

$$\langle\tilde{k}, u\rangle = \left\langle \frac{\mathrm{d}x}{\mathrm{d}\lambda}, u \right\rangle = \frac{\mathrm{d}x^0}{\mathrm{d}\lambda} = \frac{c\mathrm{d}t}{\mathrm{d}\lambda} = 1 + z = a^{-1}. \tag{3.29}$$

Using the relation between conformal and cosmic time we can write $\mathrm{d}\lambda = ac\mathrm{d}t = a^2\mathrm{d}\eta$ and can express the Jacobi equation for the homogeneous background as

$$\nabla^2_{\tilde{k}} v^i = \frac{\mathrm{d}^2 v^i}{\mathrm{d}\lambda^2} = \mathcal{T}^i_{\mathrm{bg}\ j} v^j = \mathcal{R} v^i \tag{3.30}$$

where we have used that the basis vectors of the perpendicular screen are parallel transported along the light ray. Since $\mathrm{d}s = 0$ for light, we can express $\mathrm{d}\lambda$ by $\mathrm{d}w$ using that $\mathrm{d}w = \mathrm{d}\eta = a^{-2}\mathrm{d}\lambda$ and can conclude $\mathrm{d}\lambda = a^2\mathrm{d}w$. Now we introduce comoving bundle dimensions v^i/a for the fiducial ray and can express the propagation with the comoving distance by

$$\frac{\mathrm{d}^2}{\mathrm{d}w^2}\left(\frac{v^i}{a}\right) = a^2\frac{\mathrm{d}}{\mathrm{d}\lambda}(v^{i\prime}a - v^i a') = a^2(v^{i\prime\prime}a - v^i a'') \tag{3.31}$$

where the primes denote the derivative with respect to λ. Together with the relation $\mathrm{d}\lambda = ac\mathrm{d}t$ we can calculate the derivatives

$$a' = \frac{\mathrm{d}a}{\mathrm{d}\lambda} = \frac{1}{ca}\frac{\mathrm{d}a}{\mathrm{d}t} = \frac{\dot{a}}{ca}, \tag{3.32}$$

$$a'' = \frac{\mathrm{d}a'}{\mathrm{d}\lambda} = \frac{1}{ac}\frac{\mathrm{d}a}{\mathrm{d}t}\frac{\mathrm{d}a'}{\mathrm{d}a} = \frac{1}{c^2}\frac{\dot{a}}{a}\frac{\mathrm{d}}{\mathrm{d}a}\frac{\dot{a}}{a} = \frac{1}{2c^2}\frac{\mathrm{d}}{\mathrm{d}a}\left(\frac{\dot{a}}{a}\right)^2. \tag{3.33}$$

The $(\dot{a}/a)^2$ term can be replaced with the help of Friedmann's equation and the cosmological-constant term vanishes because $\tilde{k}$ is a null vector. The second derivative then reads

$$a'' = -\frac{4\pi G}{c^2}\frac{\rho_0}{a^4} + \frac{K}{a^3} \tag{3.34}$$

and can be inserted into the propagation equation. Using equation 3.28 and 3.30 we can express the propagation equation for the comoving light bundle in the Friedmann-Lemaître-Robertson-Walker metric by

$$\frac{\mathrm{d}^2}{\mathrm{d}w^2}\left(\frac{v^i}{a}\right) = a^3 v^{i\prime\prime} + \frac{4\pi G}{c^2}\frac{\rho_0}{a^2}v^i - K\frac{v^i}{a} = -K\frac{v^i}{a} \tag{3.35}$$

or in a more simple form

$$\left(\frac{\mathrm{d}^2}{\mathrm{d}w^2} + K\right)\frac{v^i}{a} = 0 \tag{3.36}$$

which has a very intuitive interpretation: If there is no curvature, the bundle dimension will linearly increase according to its initial angle. If the curvature is negative, we have an exponential solution and the light rays will drive apart on this hyperbolic manifold. But if the curvature is positive, we have oscillatory solutions which represent the case where we sent out two light rays at the north pole with a certain initial angle to each other and they meet again at the south pole due to curvature of the sphere.

3.2.4 Inhomogeneities' Contribution

We assume a perturbed Friedmann-Lemaître-Robertson-Walker metric with local inhomogeneities characterized by their gravitational potential. We still expect these perturbations to be small and their Newtonian potential is given by $\Phi = \phi c^2 \ll c^2$. The peculiar velocities of the inhomogeneities should be negligible compared to the cosmic flow and therefore we can write the perturbed line

element as

$$\mathrm{d}s^2 = a(\eta)^2\left[-(1+2\phi)\mathrm{d}\eta^2 + (1-2\phi)\left(\mathrm{d}w^2 + f_K^2(w)\mathrm{d}\Omega^2\right)\right]. \tag{3.37}$$

The spatial extent of the perturbations should be small compared to the curvature scale of the background universe. This assumption is generally valid and allows us to expand the comoving distance function to first order $f_K(w) \approx w$ for all three cases. Hence we can analyse light propagation in the comoving Newtonian metric

$$\mathrm{d}s^2 = -(1+2\phi)\mathrm{d}\eta^2 + (1-2\phi)\mathrm{d}\vec{w}^2. \tag{3.38}$$

It is convenient to introduce the dual basis

$$\theta^0 = (1+\phi)\mathrm{d}\eta, \qquad \theta^i = (1-\phi)\mathrm{d}w^i \tag{3.39}$$

in order to receive a Minkowskian representation of the metric with the signature $(-1,1,1,1)$. We perform a linear perturbation analysis and neglect all terms of $\mathcal{O}(\phi^2)$ or higher and assume ϕ to be time independent. Now we use Cartan's structure equations to calculate the Riemann and Ricci tensors. The first structure equation implies the connection forms

$$\omega_i^0 = \phi_i\theta^0, \qquad \omega_j^i = -\phi_j\theta^i + \phi_i\theta^j \tag{3.40}$$

wherein we use the abbreviation $\phi_j = \partial_j\phi$ and take all derivatives with respect to comoving Cartesian coordinates. The curvature forms

$$\Omega_i^0 = \phi_{ik}\theta^k \wedge \theta^0, \qquad \Omega_j^i = -\phi_{jk}\theta^k \wedge \theta^i + \phi_{ik}\theta^k \wedge \theta^j \tag{3.41}$$

can be calculated with Cartan's second structure equation. Thus the only non-vanishing elements of the Riemann tensor are

$$R_{0i0j} = \phi_{ij}, \quad R_{ijij} = \phi_{ii} + \phi_{jj}, \quad R_{1213} = \phi_{23}, \quad R_{1223} = -\phi_{13}, \quad R_{1323} = \phi_{12} \tag{3.42}$$

and the Ricci tensor and Ricci scalar are

$$R_{\alpha\beta} = \vec{\nabla}^2\phi 1_4, \qquad R = 2\vec{\nabla}^2\phi \tag{3.43}$$

with the notation $\vec{\nabla}^2 = \partial^i\partial_i$. The Einstein tensor hence is

$$G_{\alpha\beta} = \vec{\nabla}^2\phi\delta_\alpha^0\delta_\beta^0. \tag{3.44}$$

Now we can compute the Weyl tensor needed for the inhomogeneity contributions to the optical tidal matrix. The Weyl curvature is defined by

$$C_{\alpha\beta\gamma\delta} = R_{\alpha\beta\gamma\delta} - g_{\alpha[\gamma}R_{\delta]\beta} + g_{\beta[\gamma}R_{\delta]\alpha} + \frac{R}{3}g_{\alpha[\gamma}g_{\delta]\beta} \tag{3.45}$$

and has the only non-vanishing components

$$C_{0i0j} = \phi_{ij} - \frac{1}{3}\vec{\nabla}^2\phi\eta_{ij}, \qquad C_{ijij} = \phi_{ii} + \phi_{jj} - \frac{2}{3}\vec{\nabla}^2\phi, \tag{3.46}$$

$$C_{1213} = \phi_{23}, \qquad C_{1223} = -\phi_{13}, \qquad C_{1323} = \phi_{12}. \tag{3.47}$$

According to equation 3.20 and 3.21 we can calculate the contributions to the Weyl tensor in our comoving metric caused by local inhomogeneities

$$\mathcal{R}_{\mathrm{cl}} = -\vec{\nabla}^2\phi, \qquad \mathcal{F}_{\mathrm{cl}} = -(\phi_{11} - \phi_{22}) - 2i\phi_{12} \tag{3.48}$$

and receive for the optical tidal matrix

$$\mathcal{T}_{\mathrm{cl}} = -2 \begin{pmatrix} \phi_{11} & \phi_{12} \\ \phi_{12} & \phi_{22} \end{pmatrix} \tag{3.49}$$

or expressed in components: $(\mathcal{T}_{\mathrm{cl}})_{ij} = -2\partial_i\partial_j\phi$. Denoting $\phi^{(0)}$ as the gravitational potential passed by the fiducial ray, we can expand the potential gradient as

$$\partial_i \left(\phi - \phi^{(0)}\right) = \partial_i \delta\phi = \partial_j \partial_i \phi \Big|_0 x^j = -\frac{1}{2}(\mathcal{T}_{\mathrm{cl}})_{ij} x^j. \tag{3.50}$$

This expansion allows us to write the Jacobi equation for the clump contributions in the form

$$\frac{\mathrm{d}^2 x^i}{\mathrm{d}\lambda^2} = \frac{\mathrm{d}^2 x^i}{\mathrm{d}w^2} = -2\partial^i \delta\phi. \tag{3.51}$$

We are still allowed to gauge the potential properly because the absolute value of the gravitational potential has no invariant meaning and therefore we can just set $\delta\phi = \phi$. Finally we have to keep in mind that the bundle dimensions x^i evaluated in the local frame are comoving bundle dimensions v^i/a in the cosmological frame. Now we can combine the global, homogeneous (equation 3.36) and the local clump contribution (equation 3.51) to find the inhomogeneous propagation equation for the comoving bundle dimension x^i

$$\left(\frac{\mathrm{d}^2}{\mathrm{d}w^2} + K\right) x^i = -2\partial^i \phi. \tag{3.52}$$

This linear differential equation with the inhomogeneity $-2\partial^i\phi$ caused by local perturbations allows us to describe light propagation in a very general way.

3.3 Lensing Properties

3.3.1 Lensing Potential

In a next step we want to analyse the solutions and derive an equation for the effective lensing potential which is a fundamental tool to study gravitational lenses. The differential operator $\mathrm{d}^2/\mathrm{d}w^2 + K$ is solved by the Green's function

$$\begin{aligned} G(w, w') &= \frac{1}{\sqrt{K}} \sin\left(\sqrt{K}(w - w')\right) \Theta(w - w') \\ &= f_K(w - w')\Theta(w - w') \end{aligned} \tag{3.53}$$

with the previously defined comoving angular diameter distance $f_K(w)$. We assume two light rays starting simultaneously at the same point where they enclose the angle (θ^1, θ^2). That defines the initial conditions at the observer $(w = 0)$ for the Green's function

$$x^i\Big|_{w=0} = 0, \qquad \frac{\mathrm{d}x^i}{\mathrm{d}w}\Big|_{w=0} = \theta^i. \tag{3.54}$$

Thus, the solution for the propagation of the bundle dimension is

$$x^i(w) = f_K(w)\theta^i - 2\int_0^w \mathrm{d}w' f_K(w - w')\partial^i\phi(x^j(w'), w'). \tag{3.55}$$

As we are dealing with small gravitational potentials, the deflection angle is small and we can integrate along the unperturbed light path $x^i(w') \approx f_K(w')\theta^i$ (Born's approximation). The observer is at the position $w = 0$, the source at the comoving radial distance w_s and we can define

$x^i(w_s) = f_K(w_s)\beta^i$ which gives us

$$\beta^i = \theta^i - 2\int_0^{w_s} \mathrm{d}w' \frac{f_K(w_s - w')}{f_K(w_s)} \partial^i \phi\left(f_K(w')\theta^j, w'\right). \tag{3.56}$$

Defining the reduced deflection angle

$$\alpha^i(\theta^j) = 2\int_0^{w_s} \mathrm{d}w' \frac{f_K(w_s - w')}{f_K(w_s)} \partial^i \phi\left(f_K(w')\theta^j, w'\right) \tag{3.57}$$

we obtain the lens equation

$$\beta^i = \theta^i - \alpha^i(\theta^j). \tag{3.58}$$

Now we introduce derivatives with respect to angular coordinates θ^j on the sky

$$\partial_x = \frac{\partial_\theta}{f_K(w)} \tag{3.59}$$

which have to be interpreted as covariant derivatives on the sphere if the curvature is not negligible. For later purposes it is convenient to write the reduced deflection angle as the angular gradient of an effective lensing potential

$$\psi(\theta^j) = 2\int_0^{w_s} \mathrm{d}w' \frac{f_K(w_s - w')}{f_K(w')f_K(w_s)} \phi\left(f_K(w')\theta^j, w'\right). \tag{3.60}$$

The lensing potential can be specialised to different lens models and is a very powerful tool to study the behaviour of lens mapping as we will see later on. The deflection angle then reads

$$\alpha^i = \partial_i \psi \tag{3.61}$$

and we can introduce the convergence κ as the Laplacian of the lensing potential

$$\kappa = \frac{1}{2}\partial^i \partial_i \psi \tag{3.62}$$

and write it in the general form

$$\kappa(x^j) = \int_0^{w_s} \mathrm{d}w' \frac{f_K(w_s - w')f_K(w')}{f_K(w_s)} \partial_{x^i}\partial^{x^i} \phi(x^j, w'). \tag{3.63}$$

We will understand the meaning and utility of the convergence later on but for the moment we need it to apply Poisson's equation. Using Poisson's equation

$$\nabla^2 \phi = \frac{4\pi G}{c^2}\rho \tag{3.64}$$

we can express the convergence by the local density ρ

$$\kappa(\theta^j) = \frac{4\pi G}{c^2}\int_0^{w_s} \mathrm{d}w' \frac{f_K(w_s - w')f_K(w')}{f_K(w_s)} \rho(f_K(w')\theta^i, w'). \tag{3.65}$$

3.3.2 Lens Geometry

For a gravitational lens system we need a source, a mass distribution acting as a gravitational lens and an observer who is interested in this phenomenon. Usually the distances between source, lens and observer are very large compared to the spatial extent of the gravitational lens. Therefore we are allowed to use the thin-lens approximation where we assume the mass distribution to be two

dimensional in the lens plane and can use the line-of-sight projection of the Newtonian potential

$$\phi \to \delta(w - w_d) \int \mathrm{d}w' \phi = \delta(w - w_d)\tilde{\phi}. \tag{3.66}$$

The distance w_d denotes the distance from the observer to the lens. Furthermore we introduce w_s as the distance between observer and source and w_{ds} as the distance between source and lens (figure 13). From this geometry we can express the reduced deflection angle (equation 3.57) as

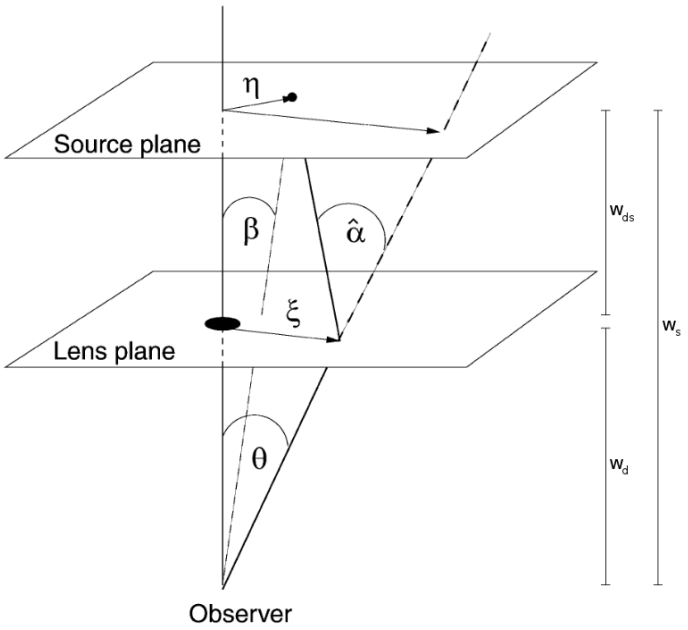

Figure 13: Geometry of a simple gravitational lens system. The comoving radial distances w_d, w_s and w_{ds} denote the distances between observer and lens, observer and source and lens and source respectively. The optical axis is defined by the line of sight from observer to the centre of the gravitational lens. The lens and source planes are perpendicular to this line of sight. The light beam intersects the lens plane at ξ and is deflected by an angle $\hat{\alpha}(\xi)$ [16].

$$\alpha(\theta) = \frac{w_{ds}}{w_s}\hat{\alpha}(w_d\theta) \tag{3.67}$$

and the lens equation using the thin lens approximation and assuming $f_K(w) = w$ yields

$$\beta^i = \theta^i - 2\frac{w_d w_{ds}}{w_s}\partial^i\tilde{\phi}(w_d\theta^j). \tag{3.68}$$

According to equation 3.65 we can express the convergence as

$$\kappa(\theta^i) = \frac{4\pi G}{c^2}\frac{w_{ds}w_d}{w_s}\int_0^{w_s} \mathrm{d}w' \rho(w'\theta^i, w') \tag{3.69}$$

and see that it is proportional to the geometrically weighted surface-mass density of the lensing mass distribution. The surface-mass density of the lens is suitably defined by the projection of the spatially extended density ρ onto the lens plane along the line-of-sight

$$\Sigma(\theta^i) = \int \mathrm{d}w' \rho(w'\theta^i, w'). \tag{3.70}$$

Defining the critical surface mass density

$$\Sigma_{\mathrm{cr}} = \frac{c^2}{4\pi G}\frac{w_s}{w_{ds}w_d} \tag{3.71}$$

we can express the convergence of a thin lens as

$$\kappa(\theta^i) = \frac{\Sigma(\theta^i)}{\Sigma_{\mathrm{cr}}}. \tag{3.72}$$

3.3.3 Lensing by a Point Mass

We want to apply our knowledge about gravitational lensing to the most simple case of a point mass acting as lens. The spatial extend of this point mass M is described by a delta function

$$\rho(\vec{x}) = M\delta(\vec{x}) \tag{3.73}$$

and the convergence turns into

$$\kappa(\vec{\theta}) = \frac{4\pi GM}{c^2}\frac{w_{ds}w_d}{w_s}\delta(w_d\vec{\theta}). \tag{3.74}$$

The lensing potential can be written in the form

$$\psi(\vec{\theta}) = \frac{4GM}{c^2}\frac{w_{ds}}{w_d w_s}\ln|\vec{\theta}| \tag{3.75}$$

from where we can derive the deflection angle

$$\vec{\alpha} = \vec{\nabla}\psi = \frac{4GM}{c^2}\frac{w_{ds}}{w_d w_s}\frac{\vec{\theta}}{\vec{\theta}^2}. \tag{3.76}$$

Inserting this into the lens equation we obtain

$$\vec{\beta} = \vec{\theta} - \frac{4GM}{c^2}\frac{w_{ds}}{w_d w_s}\frac{\vec{\theta}}{\vec{\theta}^2} \tag{3.77}$$

which is one-dimensional because of the axisymmetry of the lens. This quadratic equation is very useful to study the qualitative behaviour of the lens mapping for this simple geometry. We introduce the Einstein radius

$$\theta_E = \left(\frac{4GM}{c^2}\frac{w_{ds}}{w_d w_s}\right)^{1/2} \tag{3.78}$$

which simplyfies the equation to

$$0 = \theta^2 - \beta\theta - \theta_E^2. \tag{3.79}$$

We want to analyse the solutions and its interpretations:

- $\beta = 0$ describes the case where the source is located directly behind the lens. Observer, lens and source are on one line and the problem is axially symmetric. The lens equation has the solution $\theta = \theta_E$ which means that the source is mapped into a circular image around the lens. Such images are called Einstein rings and there are some known cases of observed Einstein rings e.g. figure 14.

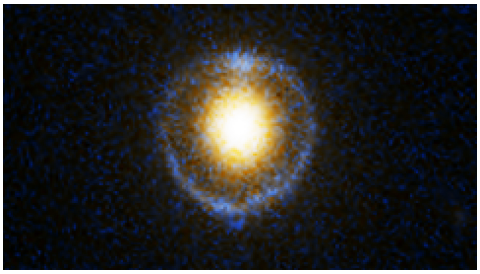

Figure 14: Einstein Ring Gravitational Lens SDSS J162746.44-005357.5: The source is almost exactly behind the lens and is seen as a circular image [25].

- $\beta \neq 0$ is the most general case and we expect two solutions which are collinear with the lens and the source. These two images are at the positions $\theta_{\pm} = \frac{1}{2}\left(\beta \pm \sqrt{\beta^2 + 4\theta_E^2}\right)$. One of the images is located on the same side of the lens as the source and the second image is located on the other side (Figure 15).

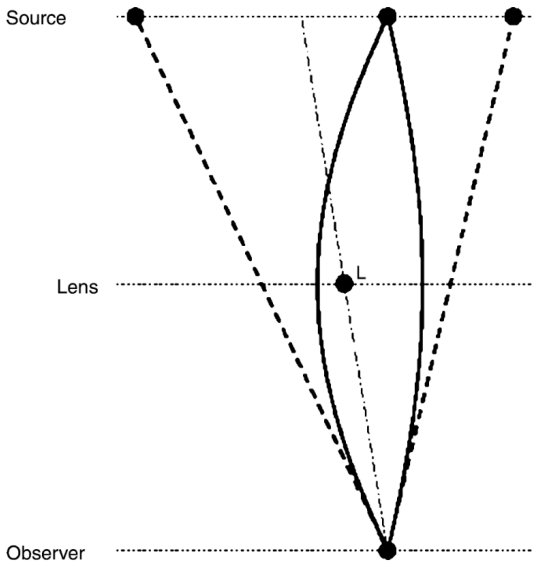

Figure 15: Sketch of a gravitational lens system with a point mass located at L. If the mass is sufficiently large we might be able to observe 2 images of the original source [14].

- $\beta \gg \theta_E$ describes the situation where the influence of the gravitational lens is negligible but formally we have two solutions at $\theta_1 \approx 0$ and $\theta_2 \approx \beta$. The first solution is not observable because it is too faint (see later) and located behind the lens whereas the second solution represents the unperturbed position of the original source.
- All of these cases are summarized in figure 16 where we can see the behaviour for small and large β and for the general case in between.

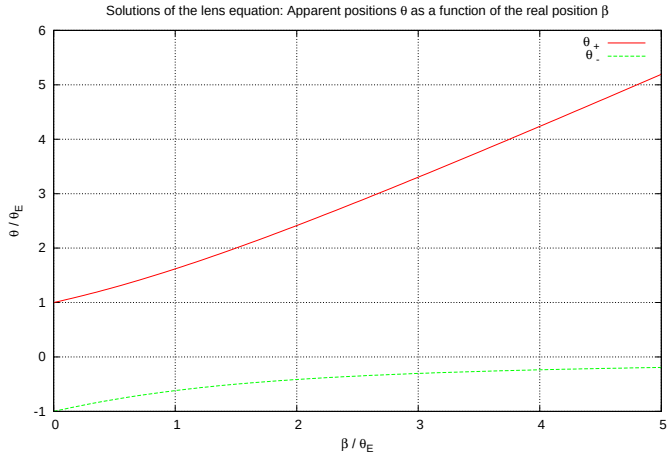

Figure 16: Apparent positions of the source as a function of the real position. All angles are scaled by the Einstein radius θ_E. For $\beta = 0$ the source is seen as a circular image which is called the Einstein ring. For $\beta \gg \theta_E$ the function turns towards the identity function and for moderate values of β we have two solutions at different sides of the lens.

So far we have seen the lensing properties of a point mass lens. This is the simplest lens model but it already reveals some interesting characteristics of gravitational lensing. To understand more complex lensing systems, we have to study the local lensing properties (magnification, convergence, shear) and the different mass distributions in detail.

3.3.4 Magnification

Light beams coming from the source to us are bundles of rays with a certain cross section. This cross section of a bundle is differentially deflected and therefore geometrically distorted: Rays passing closer to the lens are more deflected than those rays of the bundle which are passing farther away. Liouville's theorem and the absence of emission or absorption of photons imply that lensing conserves the specific intensity I_ν and therefore the surface brightness. Hence, magnification arises only because the lens mapping changes the solid angle under which the source appears. The observed flux is the product of surface brightness and solid angle but as the surface brightness is conserved, the flux changes according to the solid angle. Let ω_s be the solid angle, the source would subtend if no lens was present and ω the observed solid angle of the image. The magnification is then given by

$$\mu := \frac{\omega}{\omega_s} \tag{3.80}$$

The magnification can be calculated by the differential area distortion of the lens mapping

$$\mu = \frac{\theta}{\beta}\frac{\mathrm{d}\theta}{\mathrm{d}\beta} = \left|\det\left(\frac{\partial\beta^i}{\partial\theta^j}\right)\right|^{-1}. \tag{3.81}$$

We can now determine the magnification for each individual image

$$\mu_\pm = \left[1 - \left(\frac{\theta_E}{\theta_\pm}\right)\right]^{-1} = \frac{u^2+2}{2u\sqrt{u^2+4}} \pm \frac{1}{2} \tag{3.82}$$

where we have introduced $u = \beta/\theta_E$ as the position scaled by the Einstein radius. The total magnification can be expressed by adding the two contributions

$$\mu = \mu_+ + \mu_- = \frac{u^2+2}{u\sqrt{u^2+4}}. \tag{3.83}$$

The magnification is always positive but nevertheless, the determinant of the Jacobi matrix may have either sign. The concept of parity defines the orientation of the lensed image with respect to the image in the source plane and the sign of $\det(\partial\beta^i/\partial\theta^j)$ determines the associated parity: Images of the source for which the determinant is positive (negative) are said to posses positive (negative) parity. But it is also possible, that a source has images for which the determinant vanishes. These locations in the lens plane are called critical curves and they separate regions of different parity. According to equation 3.81 the magnification factor formally diverges on these critical curves. However this divergence does not cause an infinitely magnified source because we have to consider two additional effects:

- Real sources are extended and the actual magnification is the weighted mean which is always a finite value.
- Even for point-like sources the magnification is bounded, because the assumptions of geometrical optics are no longer valid and we also have to consider interference effects.

The lens equation directly relates positions in the lens plane to positions in the source plane. If we thus know the location of the critical curves, we can calculate the associated locations in the source plane, which are called caustics. The concept of critical curves and caustics is very important to understand the qualitative behaviour of lens mapping: "The number of images changes by two if and only if the source crosses a caustic" [26] which is valid for gravitational lenses with a smooth surface mass density. Depending on the direction of crossing, two images with opposite parity merge into one image on the critical curve and then disappear or vice versa. Figure 17 shows an example for critical lines and caustic of a non-singular, circularly symmetric lens. Magnification is an important tool for the observation of gravitationally lensed images because astrometry gets

preciser the brighter the images are. But as we will see later on, we can not just choose the brightest images for the determination of H_0 because we also have to fulfill additional geometrical criteria. The partial derivatives in equation 3.81 can also be written as

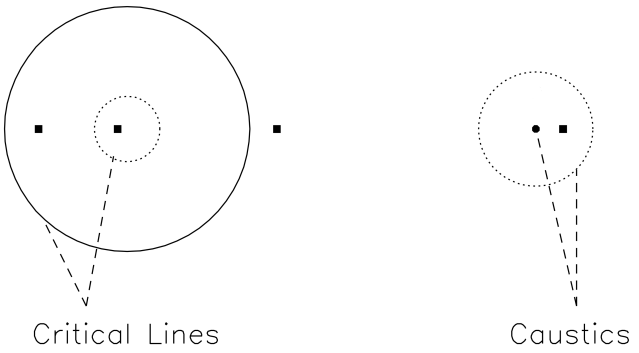

Figure 17: Imaging of a point source by a non-singular, circularly symmetric lens. Left: image positions and critical lines; right: source position and corresponding caustics [15].

$$\frac{\partial \beta^i}{\partial \theta^j} = \delta^i_j - \frac{\alpha^i}{\theta^j} = \delta^i_j - \frac{\partial^2 \psi}{\partial \theta_i \partial \theta^j} = \delta^i_j - \psi^i_j \tag{3.84}$$

using the lens equation and the definition of the lensing potential. We can separate this matrix into its trace and trace-free part

$$\frac{\partial \beta^i}{\partial \theta^j} = \begin{pmatrix} 1-\kappa & 0 \\ 0 & 1-\kappa \end{pmatrix} - \begin{pmatrix} \gamma_1 & \gamma_2 \\ \gamma_2 & -\gamma_1 \end{pmatrix} \tag{3.85}$$

where κ is the convergence defined in equation 3.62 and

$$\gamma_1 = \frac{1}{2}(\psi^1_1 - \psi^2_2), \qquad \gamma_2 = \psi^1_2 = \psi^2_1 \tag{3.86}$$

are the components of the shear

$$\gamma = \gamma_1 + i\gamma_2. \tag{3.87}$$

Now, we are able to express the magnification by the convergence and the shear components

$$\mu = \frac{1}{(1-\kappa)^2 - {\gamma_1}^2 - {\gamma_2}^2} \tag{3.88}$$

and we will need this relation later on as one way to break the so called mass-sheet degeneracy.

3.3.5 Time Delay

Generally we observe multiple images of one source but the light travel time along the rays are different. This time delay between multiple images has two reasons: First, the individual rays are deflected by different angles and therefore their geometrical lengths are different. Second, the light rays are retarded by the gravitational potential of the lens which is known as the Shapiro delay:

- **Geometrical Time Delay:** According to figure 18 we can express the distance w_{ds} from the source to the deflector with the help of the cosine law

$$w^2_{ds} = w^2_s + w^2_d - 2w_s w_d \cos(\theta - \beta) \approx (w_s - w_d)^2 + w_s w_d (\theta - \beta)^2 \tag{3.89}$$

  using the first-order Taylor expansion of the cosine in the second step. Furthermore we can

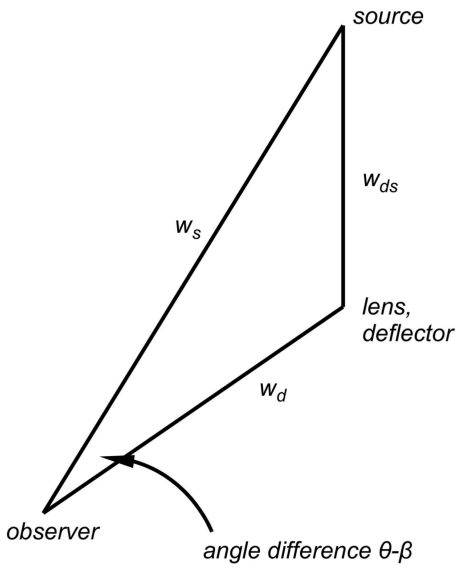

Figure 18: Illustration of the geometrical length difference of the deflected and undeflected light paths. The total difference can be expressed by the angle difference $\theta - \beta$ [13].

approximate

$$w_{ds} \approx w_s - w_d + \frac{w_s w_d}{2(w_s - w_d)}(\theta - \beta)^2 \tag{3.90}$$

and invert the equation to write

$$w_s - w_d \approx w_{ds} - w_d w_s (\theta - \beta)^2. \tag{3.91}$$

The comoving geometrical distance between the deflected and the undeflected path lengths is thus

$$\Delta w = w_d + w_{ds} - w_s \approx \frac{w_s w_d}{2(w_s - w_d)}(\theta - \beta)^2 \approx \frac{w_s w_d}{w_{ds}} \frac{(\theta - \beta)^2}{2} \tag{3.92}$$

where we have neglected terms of the order $\mathcal{O}([\theta - \beta]^4)$. The geometrical time delay can hence be written as

$$\Delta t_{\mathrm{geo}} = \frac{\Delta w}{c} = \frac{w_s w_d}{w_{ds} c} \frac{(\theta - \beta)^2}{2}. \tag{3.93}$$

- **Gravitational Time Delay:** The Shapiro delay was first observed in 1964 by I. I. Shapiro [27]. Due to a time dilatation of the photons, electromagnetic waves passing a strong gravitational field take longer to travel to a target than they would take without the presence of a gravitational field. This gravitational time delay can generally be calculated by

$$\Delta t_{\mathrm{grv}} = -2 \int_{\mathrm{source}}^{\mathrm{observer}} \mathrm{d}w' \frac{\phi(\theta w', w')}{c} \tag{3.94}$$

or in terms of the lensing potential

$$\Delta t_{\mathrm{grv}}(\theta) = -\frac{1}{c} \frac{w_s w_d}{w_{ds}} \psi(\theta) \tag{3.95}$$

The two contributions of the time delay can be added to derive an expression for the total time delay

$$\Delta t(\theta) = \frac{1}{c} \frac{w_s w_d}{w_{ds}} \left(\frac{(\theta - \beta)^2}{2} - \psi(\theta) \right). \tag{3.96}$$

According to Fermat's principle, the light-travel time is stationary for the actual trajectory of the light ray compared to neighbouring trajectories. The stationarity of light-travel time can be

expressed by

$$\partial_i \Delta t = 0. \tag{3.97}$$

If the source is far away from the lens, one image is formed. Further images are formed in pairs as the source moves behind the lens and therefore the total number of images is odd. This odd-number theorem is not valid for all observations, because images might be merged together, loacted behind the lens or just to faint to be observable. The time delay function depends on observable quantities as the distances of source and lens or the lensing potential which can be calculated for various lens models. The comoving radial distances w depend on the redshift according to equation 2.25. This integral might be difficult to solve for a given cosmological model but in any case the relation

$$w \propto \frac{1}{H_0} \tag{3.98}$$

is valid. This leads to a very fundamental conclusion for this thesis: The time delay is proportional to the inverse of the Hubble constant

$$\Delta t \propto \frac{1}{H_0}. \tag{3.99}$$

Turning this argument around, we are able to determine Hubble's constant based on observable quantities. In section 4 we will see in detail, what these quantities are and how to determine them.

3.3.6 Mass-Sheet Degeneracy and its Elimination

To determine the Hubble constant we have to find a suitable mass model of the lens which reproduces the observations and leads to an effective lensing potential. Possible lens models are a point mass, a singular isothermal sphere, a non-singular isothermal sphere, or elliptical models and will be discussed in detail later on. One can ask now, if such a model of the mass distribution is unique. In 1985 Falco et al. discovered, that there exists a transformation which leaves the observable images unchanged but creates a family of different mass distributions. This invariance leaves the relation between the intrinsic and observed ellipticity unchanged and therefore it can not be broken by just using measurements of the distortion of the background sources. This transformation and the connected ambiguity is known as the mass-sheet degeneracy:
The observable data (image position, flux ratios, image shapes,...) are best fit by the mass distribution $\kappa(\theta)$. The transformation

$$\kappa_\lambda(\theta) = (1-\lambda) + \lambda\kappa(\theta) \tag{3.100}$$

then creates a band of equally good fits to the data which can be shown by inserting into the lens equation

$$\begin{aligned} \beta &= \theta - \alpha_\lambda(\theta) \\ &= \theta - ((1-\lambda)\theta + \lambda\alpha(\theta)) \end{aligned} \tag{3.101}$$

where quantities with the index λ correspond to the scaled mass distribution $\kappa_\lambda(\theta)$. Furthermore we have to satisfy

$$\alpha_\lambda(\theta) = \nabla\psi_\lambda(\theta) \tag{3.102}$$

with

$$\psi_\lambda(\theta) = \frac{1-\lambda}{2}|\theta|^2 + \lambda\psi(\theta) \tag{3.103}$$

and the Poisson equation

$$\nabla^2\psi_\lambda = 2\kappa_\lambda. \tag{3.104}$$

Combining these equations we receive the transformed lens equation

$$\frac{\beta}{\lambda} = \theta - \alpha(\theta) \tag{3.105}$$

for the mass distribution κ_λ which has the same form as the untransformed equation up to a scaling factor λ^{-1} which is not directly observable. The second term in our original transformation describes a rescaling of the mass distribution $\kappa(\theta)$ and the first term can be related to a homogeneous surface mass density $\kappa_h = 1 - \lambda$ which is added to the scaled original mass density and explains the name of this degeneracy.
As the mass distribution κ is not uniquely defined, nor is the lensing potential ψ. But to calculate ψ and derive a value for H_0 we have to find an independent way of breaking this mass-sheet degeneracy. There are different possible methods for doing so:

- The time delay Δt is proportional to the difference in the lensing potential calculated at two different image positions and therefore is changed by this transformation. Generally, we can use the value of Hubble's constant from other cosmological observations to break the mass sheet degeneracy but as we are interested in calculating H_0 independently, this method is not suitable for our purpose.

- The critical surface density Σ_{cr} depends on the lens geometry as well as on the distances between source, lens and observer. If we are able to detect sources at different distances w_{s1} and w_{s2} deflected by the same lens, the resulting convergence $\kappa = \Sigma/\Sigma_{\mathrm{cr}}$ will be different for the individual sources. The mass-sheet degeneracy can be broken by this additional information of a second lensed source but unfortunately, the possibility for such an event is very low.

- As we see in equation 3.105 the source position β is not invariant under the mass-sheet transformation. Generally we are not able to observe β, unless the lens moves relatively to the source. A time dependent lens system might provide the information of the lensed and unlensed source and with the help of this additional information we can eliminate the mass-sheet degeneracy.

- The convergence and shear transform as

$$1 - \kappa_\lambda = \lambda(1 - \kappa), \qquad \gamma_\lambda = \lambda\gamma \tag{3.106}$$

  and thus the magnification transforms according to

$$\mu_\lambda = \frac{1}{(1-\kappa_\lambda)^2 - {\gamma_\lambda}^2} = \frac{1}{\lambda^2}\frac{1}{(1-\kappa)^2 - \gamma^2} \propto \lambda^{-2}. \tag{3.107}$$

  In order to break the mass-sheet degeneracy, we have to find an independent way of measuring the relative magnification of the images. One method uses the fact, that gravitational lensing conserves the surface brightness and if we know the original size of the galaxy we can calculate the magnification. The size of elliptical galaxies can be determined statistically, based on the velocity dispersion and the surface brightness (which are both independent of gravitational lensing) with the help of the fundamental plane. The other method is based on two effects of gravitationally lensed fields: on the one hand the number of observable galaxies increases because of the magnification. On the other hand the number of galaxies per solid angle decreases because the solid angle is stretched due to the lens mapping. By quantifying these two effects with the help of empirical estimations for the logarithmic slope of the intrinsic number count function, one can calculate the magnification and break the mass sheet degeneracy.

All these methods can help us to break or at least constrain the mass-sheet degeneracy. But even without knowing about the exact value of our transformation parameter λ, we know that only certain values for λ are physically meaningful. The non-negativity of the surface mass-sheet density restricts possible values of λ and consequently possible values of H_0.

3.4 Lens Models

So far, we have only assumed point masses as gravitational lenses. This simple model is very useful to study the general behaviour and effects of gravitational lensing, but in order to study real mass distributions and calculate their lensing potentials, we have to consider further mass models. As Newtonian gravity is linear, we can just superpose the mass distributions or associated lensing potentials to derive more complex models. In this chapter we want to discuss the most prominent lens models which can be used to fit the observed data.

3.4.1 Singular Isothermal Sphere (SIS)

We are mainly interested in gravitational lensing by galaxies and therefore we have to find a way to describe the mass and density distribution in a galaxy. The most prominent model is a SIS where we assume an equation of state to describe the single stars thermodynamically like gas particles and the Euler equation to derive a density profile. These assumptions are generally justified but we have to keep in mind that this is still an idealised model which has to be modified later on. We start from the equation of state

$$p = \frac{\rho k_B T}{m} \tag{3.108}$$

where p is the pressure, ρ is the density, m is the mass of a single star and T is the associated temperature which is assumed to be constant in the galaxy. The mass of each star in the galaxy should be the same and we can relate the velocity dispersion σ to the temperature

$$m\sigma^2 = k_B T. \tag{3.109}$$

As the temperature is homogeneous in the galaxy, so is the velocity dispersion. The problem is spherically symmetric and we can simplify Euler's equation

$$\frac{\vec{\nabla} p}{\rho} = -\frac{GM(r)}{r^2}\vec{e}_r \tag{3.110}$$

to a one dimensional problem with the radial distance as remaining coordinate. Using the equation of state we can integrate Euler's equation to derive one solution for the density profile

$$\rho(r) = \frac{\sigma^2}{2\pi G}\frac{1}{r^2} \propto r^{-2}. \tag{3.111}$$

This density distribution reproduces the flat rotation curves of galaxies and σ can simply be measured with the help of spectroscopy through line widths. In many cases this simple model reproduces the lensing properties very well. The surface mass density is the projection along the line of sight and can be calculated to be

$$\Sigma(\xi) = \frac{\sigma^2}{2G\xi} \tag{3.112}$$

with the radial distance ξ. The projected mass enclosed by the radius r can be expressed by

$$M(r) = 2\pi \int_0^r \mathrm{d}\xi \Sigma(\xi)\xi = \frac{\pi\sigma^2 r}{G} \tag{3.113}$$

and we obtain the lensing potential

$$\psi = 4\pi \left(\frac{\sigma}{c}\right)^2 \frac{w_{ds}}{w_s} |\vec{\theta}|. \tag{3.114}$$

The deflection angle of a SIS

$$\vec{\alpha}_0 = 4\pi \left(\frac{\sigma}{c}\right)^2 \frac{w_{ds}}{w_s} \frac{\vec{\theta}}{|\vec{\theta}|} \tag{3.115}$$

is obviously independent of θ. If $|\beta| < \alpha_0$ we expect two solutions whose separation is of the order of arcseconds and independent of θ. The magnification of a SIS is given by

$$\mu(\theta) = \left| \frac{\theta/\alpha_0}{\theta/\alpha_0 - 1} \right|. \tag{3.116}$$

This model is suitable for many lenses but it needs further modifications in order to describe more complex mass distributions.

3.4.2 Non-Singular Isothermal Sphere

Obviously, the SIS can not be a physically correct model because the density might diverge for $r \to 0$ and the total mass might be infinite without a defined outer bound of the galaxy. The outer bound can be chosen according to the size of the galaxy and the diverging density can be corrected by introducing a core radius r_c with the associated density profile of the non-singular isothermal sphere

$$\rho(r) = \frac{\sigma^2}{2\pi G} \frac{1}{r^2 + r_c^2}. \tag{3.117}$$

Defining the angular core radius $\theta_c = r_c / w_d$ we can derive the surface mass density

$$\Sigma(\theta) = \frac{\sigma^2}{2G w_d} \frac{1}{\sqrt{\theta_c^2 + \theta^2}}. \tag{3.118}$$

Therefore the convergence is given by

$$\kappa(\theta) = \frac{\kappa_0}{2\sqrt{\theta_c^2 + \theta^2}} \tag{3.119}$$

with

$$\kappa_0 = 4\pi \frac{\sigma^2}{c^2} \frac{w_{ds}}{w_s}. \tag{3.120}$$

If the angle θ is much larger than the angular core radius $\theta \gg \theta_c$ the effective lensing potential

$$\psi(\theta) = \kappa_0 \left(\sqrt{\theta_c^2 + \theta^2} - \theta_c \ln \frac{\theta_c + \sqrt{\theta_c^2 + \theta^2}}{\theta} \right) \tag{3.121}$$

can be approximated by

$$\psi(\theta) \approx 2\kappa_0 \sqrt{\theta_c^2 + \theta^2}. \tag{3.122}$$

The deflection angle

$$\alpha(\theta) = \frac{\kappa_0 \sqrt{\theta_c^2 + \theta^2}}{\theta} \tag{3.123}$$

is independent of θ for vanishing θ_c. Typical images of a non-singular isothermal sphere can be seen in figure 19.

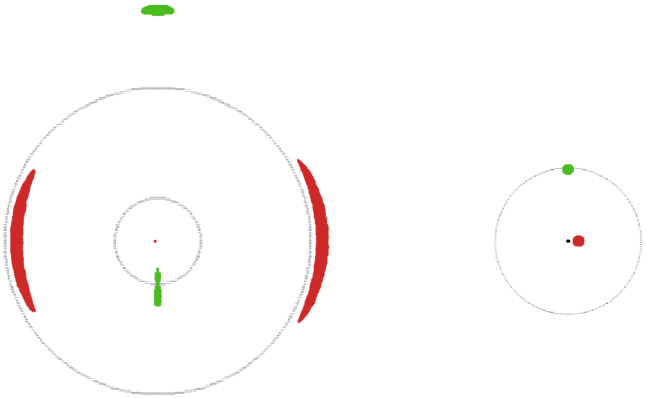

Figure 19: Two extended sources lensed by a non-singular isothermal sphere. The left image shows the lensed image positions with critical curves and the right image shows the original position of the sources with the caustics. The inner source is located close to the line of sight and is mapped onto two long tangentially oriented arcs and a faint image at the centre, whereas the outer source is imaged onto a radially elongated image which consists of two merging images and a third tangentially oriented image [15].

3.4.3 Constant Matter Sheet and Constant Shear

- It can be useful to consider a sheet of constant density in order to describe external mass distributions. The matter sheet of constant convergence κ_0 has the lensing potential

$$\psi(\theta) = \frac{\kappa_0}{2}\theta^2. \tag{3.124}$$

- Furthermore we can consider the case of vanishing convergence but constant shear created by external mass distributions. The lensing potential is given by

$$\psi(\theta) = \frac{\gamma_1}{2}(\theta_1^2 - \theta_2^2) + \gamma_2\theta_1\theta_2. \tag{3.125}$$

Combining these two lensing potentials we can model the environment like clusters or dark matter halos of the lens. The lensing potential

$$\psi(\theta_1, \theta_2) = \frac{\kappa}{2}(\theta_1^2 + \theta_2^2) + \frac{\gamma}{2}(\theta_1^2 - \theta_2^2) \tag{3.126}$$

is very useful to describe the surroundings of a lens and to introduce external effects.

3.4.4 Elliptical Lens Model

If the lensing galaxy itself is not circularly symmetric, we have to develop further models for the mass distribution and lensing potential in order to model the observations. We assume a galaxy with elliptical isodensity contours which is in agreement with real matter distributions in galaxies. The surface mass density can be described by

$$\Sigma(\theta_1, \theta_2) = \frac{1}{\sqrt{\theta_c^2 + (1-\epsilon)\theta_1^2 + (1+\epsilon)\theta_2^2}} \tag{3.127}$$

with the ellipticity ϵ, the angular core radius θ_c and the orthogonal coordinates θ_1 and θ_2. This model has analytical solutions only for some special cases. Therefore it is more convenient and still sufficient to use the elliptical effective lensing potential

$$\psi(\theta_1, \theta_2) = \frac{w_{ds}}{w_s} 4\pi \left(\frac{\sigma}{c}\right)^2 \sqrt{\theta_c^2 + (1-\epsilon)\theta_1^2 + (1+\epsilon)\theta_2^2} \tag{3.128}$$

which fits the real lenses remarkably well for small ϵ. If we deal with non-circular lenses, the image, lens and source do not necessarily have to lie on a line and we can not analyse the system as a one dimensional problem. The one dimensional time delay function has to be replaced by a two dimensional time delay surface for an elliptical lens model. The mapping of a non-singular isothermal sphere can be seen in figure 20. All these models can be used to describe the grav-

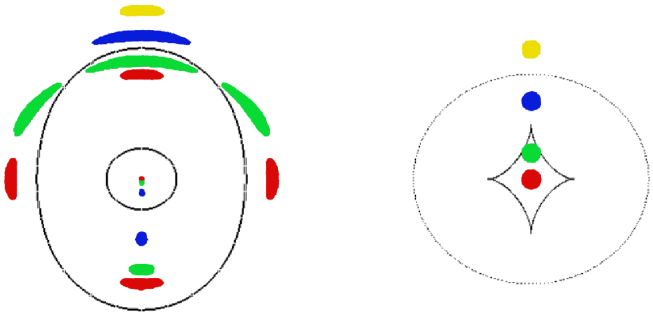

Figure 20: Lensing by an elliptical lens of a source which is moving from the optical axis outwards. The left image shows the lensed image positions with the critical curves and the right image shows the original position of the source with the caustics [15].

itational lenses and their environment. According to the required accuracy we can choose even more sophisticated models, but in most cases the presented models and their superpositions are sufficient for our purposes.

4 Measuring Hubble's Parameter by Gravitational Lensing

Gravitational lensing is a well known effect and many lenses are observed. But among all these lensing effects there are only a few that produce multiple images of time dependent sources. If the lensed source shows a characteristic time dependent behaviour (e.g. supernova explosion), the information does not reach us simultaneously, but with a certain time difference Δt between the single lensed images. As we have seen in the previous section, this time delay can be used to measure the Hubble constant. But in order to do so, we need information on the image positions, magnification, cosmological parameters, redshifts and especially the lens' mass distribution. In this chapter, we want to describe observable quantities and how to derive the essential lensing parameters. Furthermore we investigate the errors and their relative influence on the value of H_0. This analysis enables us to distinguish between important parameters which should be measured more precisely and other parameters, which have a negligible influence on Hubble's parameter. At the end of this chapter we study the quadruple gravitational lens B1608+656 regarding its mass model dependence and the influence of measurement uncertainties.

4.1 Refsdal's Proposal

In 1964 S. Refsdal published a paper "on the possibility of determining Hubble's parameter [...] from the gravitational lens effect" [23]. Although no gravitational lens had been observed at that time, the theory on gravitational lensing prospered. Refsdal based his theory on simplified assumptions and obtained a reasonable expression for H_0 depending on observational parameters. He assumed the lensing galaxy to be spherically symmetric and the redshift of lens and source to be small. Hence he was able to use the linear distance-redshift relation and derived an expression for Hubble's parameter

$$H_0 = \frac{z_s z_d {\alpha_{12}}^2}{\Delta t (z_s - z_d)} \frac{\sqrt{L_1/L_2} - 1}{\sqrt{L_1/L_2} + 1} \tag{4.1}$$

with the redshift of the source z_s and deflector z_d, the time difference Δt, the image separation α_{12} and the luminosities of the individual images L_1 and L_2. Refsdal admits that this model is too simple and corrections for the actual mass distribution and more suitable galaxy models are necessary. Furthermore he pointed out that the observation of such a lensing event with measurable time delay should be possible every third year. Refsdal was the first who considered this new method of determining the Hubble constant and his theoretical foundation developed during the next years. The two main aspects which had to be clarified are the model dependences and the mass sheet degeneracy with its correction [28].

4.2 What do Gravitational Lens Time Delay Measure?

The key information for measuring the Hubble constant by gravitational lensing is the time delay between different images of one source, because without any time difference there would be no possibility to determine the expansion rate. The time delay is based on the geometrical difference of the light paths on the one hand and on a time dilatation of the photons in the gravitational potential on the other hand. Therefore we want to analyse in a first step what information we can draw from the time delay Δt and we want to derive relations between the observable quantities and Hubble's parameter. This section is based on two papers by C. S. Kochanek published in the year 2002 [29] and 2003 [30] and the book "Gravitational Lensing: Strong, Weak and Micro" by P. Schneider, C. S. Kochanek and J. Wambsganss [16].

4.2.1 Analytic Models for Gravitational Lenses

First we try to find analytic solutions for the time delay function starting from axially symmetric mass distributions up to more sophisticated lens models. For simplicity we introduce the dimen-

sionless time delay

$$\tau = \frac{1}{2}(x-u)^2 + \frac{1}{2}(y-v)^2 - \psi(x,y) \tag{4.2}$$

with the angular coordinates x and y in the lens plane and the angular coordinates u and v in the source plane. The dimensionless time delay is related to our previously introduced time delay (equation 3.96) by

$$\Delta t = \frac{1}{c}\frac{w_s w_d}{w_{ds}}\tau \tag{4.3}$$

and we observe images at stationary points of the time delay

$$\nabla\tau = 0. \tag{4.4}$$

The lens produces two images at the radii R_1 and R_2 with an average radius

$$\langle R\rangle = \frac{R_1 + R_2}{2} \tag{4.5}$$

and they define an annulus of width

$$\Delta R = R_2 - R_1 \tag{4.6}$$

where we have assumed $R_2 > R_1$ without loss of generality.

Spherical Symmetric Lens: In the case of an axially symmetric mass distribution, the lensing potential depends only on the radial coordinate

$$\psi(x,y) = \psi_0(R) \tag{4.7}$$

and the two images at R_1 and R_2 lie on a line through the lens centre. The geometrical time delay between the two images can be written as

$$\Delta\tau_{geo} = \frac{1}{2}(R_2^2 - R_1^2)(1 - 2\langle\kappa\rangle) \tag{4.8}$$

where

$$\langle\kappa\rangle = \frac{2}{R_2^2 - R_1^2}\int_{R_1}^{R_2}\kappa(u)u\mathrm{d}u \tag{4.9}$$

is the average convergence in the annulus bounded by the images which represents the average surface mass density in units of the critical mass density. In order to calculate the geometrical delay we only need the derivative of the lensing potential because the Poisson equation states

$$\nabla^2\psi = 2\kappa \tag{4.10}$$

and the radial derivatives $\psi_0'(R)$ at the image positions can be expressed by

$$R_2\psi_0'(R_2) = R_1\psi_0'(R_1) + \langle\kappa\rangle(R_2^2 - R_1^2) \tag{4.11}$$

which does only depend on the potential's derivatives at the image positions. In case of an isothermal lens ($\kappa = 1/2$) the geometrical time delay vanishes. Therefore we only have to consider the gravitational time delay which depends on the surface density distribution in the annulus and the mean surface density. The total time delay is the sum of geometrical and gravitational time delay which can be expanded in a series of $\Delta R/\langle R\rangle$. Assuming that the surface density in the annulus can be described by a power law

$$\kappa = \kappa_1\left(\frac{R}{R_1}\right)^{1-\eta} \tag{4.12}$$

defined by the logarithmic slope of the density ($\rho \propto R^{-\eta}$), the time delay can be expressed as

$$\Delta\tau = (R_2^2 - R_1^2)\left((1-\langle\kappa\rangle) - \frac{1-\eta\langle\kappa\rangle}{12}\left(\frac{\Delta R}{\langle R\rangle}\right)^2 + \mathcal{O}\left(\left[\frac{\Delta R}{\langle R\rangle}\right]^4\right)\right). \tag{4.13}$$

The first term represents the exact solution for the SIS ($\eta = 2$ and $\langle\kappa\rangle = 1/2$) and the second-order correction adjusts for small changes in the Einstein radius with the shape of the density profile. For this simple model we have seen, that the time delay depends on the image positions, the average surface density in the annulus and the logarithmic slope of the density. We will see later on, how these quantities can be determined but first we want to study more complex and therefore more realistic lens models.

Axially Symmetric Lens with External Shear: Real lenses are rather non-symmetrical and in a first step we keep the concept of an axially symmetric lens but add external shear. In the analytical model we assume the external shear to be created by a quadrupole which is defined by two amplitudes and its orientation. The effects of higher order angular structures are negligibly small. If the quadrupole is generated entirely by material outside the annulus region, the quadrupole potential

$$\psi_2 = \frac{\gamma_{ext}}{2} R^2 \cos(2(\varphi - \varphi_{ext})) \tag{4.14}$$

can be expressed by the amplitude of the external shear γ_{ext} and its orientation φ_{ext}. We expect two images at the positions $(R_1\cos\varphi_1, R_1\sin\varphi_1)$ and $(R_2\cos\varphi_2, R_2\sin\varphi_2)$. This information can be used to solve for the mass inside the Einstein ring and the amplitude of the external shear. We expand the time delay in a series of $\Delta R/\langle R\rangle$

$$\Delta\tau = (R_2^2 - R_1^2)\left[T_0 + \frac{\Delta R}{\langle R\rangle}T_1 + \left(\frac{\Delta R}{\langle R\rangle}\right)^2 T_2 + \mathcal{O}\left[\left(\frac{\Delta R}{\langle R\rangle}\right)^3\right]\right]. \tag{4.15}$$

The first term

$$T_0 = (1-\langle\kappa\rangle)\sin^2\left(\frac{\Delta\varphi_{12}}{2}\right) \tag{4.16}$$

depends on the image separation $\Delta\varphi_{12} = \varphi_1 - \varphi_2$ and yields the same result as a spherically symmetric lens for collinear images ($\Delta\varphi_{12} = \pi$). The first order correction

$$T_1 = -\frac{1}{2}(1-\langle\kappa\rangle)\sin(\Delta\varphi_{12})\cot(\varphi_1 + \varphi_2 - 2\varphi_{ext}) \tag{4.17}$$

is defined by the orientation of the shear axis and vanishes for collinear images as expected for the spherical lens. The second-order correction

$$T_2 = \frac{1}{12}[-(1-\langle\kappa\rangle)(4 + 3\cos(\Delta\varphi_{12}) + \langle\kappa\rangle(\eta - 1)] \tag{4.18}$$

depends only on the surface density in the annulus. Comparing the axially symmetric lens with and without external shear, we see that new terms occur which depend only on derivatives of the monopole potential and on the mean surface mass density in the annulus.

Axially Symmetric Lens in a General Quadrupole: In a next step we want to consider the general case of a spherical mass distribution embedded in a quadrupole structure. The quadrupole potential can be split up in two shear components: the internal shear γ_{int} generated by quadrupole structures within the annulus and the external shear γ_{ext} based on the structure of the environment. Hence, the quadrupole lensing potential is given by

$$\psi_2 = \frac{1}{2}\left(\gamma_{ext}R^2 + \gamma_{int}\frac{\langle R\rangle^4}{R^2}\right)\cos(2(\varphi - \varphi_\gamma)) \tag{4.19}$$

where φ_γ denotes the shear angle. Defining the shear ratio

$$f_{int} = \frac{\gamma_{int}}{\gamma_{int} + \gamma_{ext}} \tag{4.20}$$

we can express the leading term in the time delay series as

$$T_0 = -(1 - \langle\kappa\rangle)\frac{\sin^2(\Delta\varphi_{12}/2)}{1 - 4f_{int}\cos^2(\Delta\varphi_{12}/2)} \tag{4.21}$$

which has again the expected $(1 - \langle\kappa\rangle)$ scaling. Furthermore we can see that the ratio of internal and total shear f_{int} determine the angular dependence of the time delay. It is also important to mention that the delay depends only little on the explicit structure of the quadrupole if the images are almost collinear with $\varphi_2 = \varphi_1 + \pi + \delta\varphi$, $|\delta\varphi| \ll 1$ and the expansion terms are almost identical to those for a spherical lens (equation 4.13). This means, that lensing systems with nearly collinear images are qualified best for our purpose, because uncertainties in the lens model influence the total error only on small scales. We will rediscover this statement of collinear images later in the statistical approach.

4.2.2 Semianalytic Model for Gravitational Lenses

Even the analytical model of a spherical lens in a general quadrupole is not sufficient to describe realistic lenses. Therefore we need semianalytic corrections in order to determine the complete structure of the lens' mass distribution. The spherical lens is modelled by the mass inside the average image radius and the surface density $\kappa(r)$ in the annulus between the images. It can be parametrised by the mean surface density $\langle\kappa\rangle$ and the logarithmic slope η according to $\kappa(r) \propto r^{1-\eta}$. The monopole deflection is then given by

$$\psi_0'(R) = b_0\frac{\langle R\rangle}{R} + \frac{2}{R}\int_{\langle R\rangle}^{R}\kappa(r)r\mathrm{d}r \tag{4.22}$$

where b_0 determines the mass inside $\langle R\rangle$. The monopole can be combined with a general quadrupole

$$\psi_2(R,\varphi) = \frac{1}{2}\gamma_{ext}R^2\cos(2(\varphi - \varphi_{ext})) + \frac{1}{2}\gamma_{int}\frac{\langle R\rangle^4}{R^2}\cos(2(\varphi - \varphi_{int})) \tag{4.23}$$

based on the internal and external shear components with the associated amplitudes and orientations $(\gamma_{int}, \varphi_{int})$ and $(\gamma_{ext}, \varphi_{ext})$. Now we are able to fit our semianalytic model to the observed image position: The values of b_0 and the shear components should minimize the differences in the projected source position. The remaining expressions depend on the monopole structure in the annulus, namely $\langle\kappa\rangle$ and η. These two parameters can not be determined from the available constraints and have to be specified for each individual lens. We obtain the dimensionless time delay as a function of these 2 free parameters by this fit procedure. According to Kochanek the Hubble constant can thus be expressed in the form

$$H_0 \approx A(1 - \langle\kappa\rangle) + B\langle\kappa\rangle(\eta - 1) + C \tag{4.24}$$

where the three coefficients are obtained from the fit and scale inversely with the measured time delay. The mass sheet transformation can simply be added to this model: Let κ_{ext} be the additional mass sheet and $\langle\kappa\rangle_0$ the annular surface density. Hence the convergence of this model is reduced to $\langle\kappa\rangle = (1 - \kappa_{ext})\langle\kappa\rangle_0$ and we receive a corrected expression for the Hubble constant

$$H_0 \approx (1 - \kappa_{ext})\left(A[1 - \langle\kappa\rangle_0(1 - \kappa_{ext})] + B\langle\kappa\rangle_0(\eta - 1) + C\right) \tag{4.25}$$

with the scaling $H_0 \propto (1 - \kappa_{ext})$ due to the mass sheet degeneracy.
This semianalytic approach clearly outlines the main dependences for the Hubble constant and the question "what do gravitational lens time delay measure" can be satisfactorily answered: The time delay mainly depends on the position of the lensed images and the surface density in the annulus between the images. The mean annular surface density $\langle\kappa\rangle$ is more important than its actual spatial distribution. In two-image lenses, where the images lie on opposite sides of the lens galaxy, the time delay hardly depends on the angular structure of the lens whereas the time delays of four-image lenses are very sensitive to the quadrupole structure of the potential. The semianalytic model produces simple scaling solutions for the Hubble constant that can be verified by fully numerical methods.

4.2.3 CDM Lens Model

We are interested in fixing the values of $\langle\kappa\rangle$ and η in order to obtain a value for the Hubble constant according to equation 4.24. Assuming a general lens model we try to determine these parameters based on observable quantities. Focussing on early type galaxies, the density can be modelled by the Hernquist profile

$$\rho_H(r) = \frac{M_{0H}}{2\pi} \frac{r_H}{r(r + r_H)^3} \tag{4.26}$$

with the scale length $r_H = 0.55R_e$ so that the Hernquist model locally looks like a Vaucouleurs profile with the effective radius R_e. The effective radius defines the area of the projected galaxy which emits half the luminosity and thus determines the density distribution of the visible baryons, respectively stars. The mass enclosed by the radius r in the Hernquist profile can be expressed by

$$M_H(< r) = M_{0H} \frac{r^2}{(r + r_H)^2}. \tag{4.27}$$

The galaxy's Hernquist profile is embedded into a dark matter halo. For typical halo masses, it can be described by a Navarro–Frenk–White (NFW) profile

$$\rho_N(r) = \frac{M_{vir}}{4\pi f(c)} \frac{1}{r(r + r_s)^2} \tag{4.28}$$

depending on the virial radius r_{vir}, the scale radius r_s which has to be fixed for the individual halo, the mass M_{vir} inside r_{vir} and the function

$$f(c) = \ln(1 + c) - \frac{1}{1 + c} \tag{4.29}$$

of the concentration $c = r_{vir}/r_s$. The enclosed mass in the NFW model is

$$M_N(< r) = \frac{M_{vir} f(r/r_s)}{f(c)}. \tag{4.30}$$

In order to determine the lensing properties of these potentials we have to calculate the projected surface density. Therefore it is convenient to define the function

$$\mathcal{F}(x) = \frac{1}{\sqrt{|x^2 - 1|}} \begin{cases} \arctan(\sqrt{|x^2 - 1|}) & x > 1 \\ \operatorname{arctanh}(\sqrt{|x^2 - 1|}) & x < 1 \end{cases} \tag{4.31}$$

with the normalized radial coordinate $x = R/r_H$. Based on [31] the projected surface density of the Hernquist profile can be written as

$$\Sigma_H(x) = \frac{M_{0H}}{r_H^2} \frac{(2 + x^2)\mathcal{F}(x) - 3}{2\pi(x^2 - 1)^2} = \frac{M_{0H}}{r_H^2} \hat{\Sigma}_H(x) \tag{4.32}$$

and the mass inside the radius x in the projected plane is

$$M(<x) = M_{0H}\frac{x^2(1-\mathcal{F}(x))}{x^2-1} = M_{0H}\hat{M}_H(<x). \tag{4.33}$$

In the same way we can express the surface density

$$\Sigma_N(x) = \frac{M_{vir}}{r_s^2}\frac{1-\mathcal{F}(x)}{2\pi f(c)(x^2-1)} = \frac{M_{vir}}{r_s^2}\hat{\Sigma}_N(x) \tag{4.34}$$

and the enclosed mass

$$M_N(<x) = M_{vir}\frac{\ln\left(\frac{x}{2}\right)+\mathcal{F}(x)}{f(c)} = M_{vir}\hat{M}_N(<x) \tag{4.35}$$

for the NFW-model. The virial mass and radius are connected by the relation

$$M_{vir} = \frac{4\pi}{3}\Delta_{vir}(z)\rho_u(z)r_{vir}^3 \tag{4.36}$$

with the virial overdensity $\Delta_{vir}(z)$ and the mean matter density at the lens redshift

$$\rho_u(z) = \frac{3H_0^2}{8\pi G}\Omega_0(1+z)^3. \tag{4.37}$$

These expressions can empirically be approximated by

$$\Delta_{vir}(z) \approx \frac{18\pi^2+82\xi-39\xi^2}{\Omega(z)}, \qquad \xi = \Omega(z)-1 \tag{4.38}$$

and

$$M_{vir} = 0.232\left[\frac{(1+z)r_{vir}}{100h^{-1}\mathrm{kpc}}\right]^3\left(\frac{\Omega_0\Delta_{vir}}{200}\right)10^{12}hM_\odot. \tag{4.39}$$

Furthermore the average concentration can be written as

$$c = \frac{9}{1+z}\left(\frac{M_{vir}}{8.12\cdot 10^{12}hM_\odot}\right)^{-0.14}. \tag{4.40}$$

The important statement of this derivation is, that of the total mass only the fraction

$$f_b = \frac{\Omega_{b,cold}}{\Omega_0} \tag{4.41}$$

cools to form stars. This fraction describes the ratio of baryons to the total mass of the galaxy. Hence the mass of the Hernquist profile has to be $M_{0H} = f_bM_{vir}$ and the remaining mass of the halo is $(1-f_b)M_{vir}$. The convergence can be expressed in terms of the critical surface density

$$\kappa(R) = \frac{M_{vir}}{\Sigma_c}\left[\frac{f_b}{r_H^2}\hat{\Sigma}_H\left(\frac{R}{r_H}\right)+\frac{1-f_b}{r_s^2}\hat{\Sigma}_N\left(\frac{R}{r_s}\right)\right]. \tag{4.42}$$

It depends on known or observable quantities and the cold baryon mass fraction f_b. We can now fit equation 4.42 in the annulus between the two images with a function $\kappa \propto R^{1-\eta}$. The fit provides the mean surface density in the annulus $\langle\kappa\rangle$ and the logarithmic slope η of the surface density.
This CDM model depends on empirical relations, like the expressions for the virial mass and the concentration parameter and it neglects other effects e.g. the compression of dark matter by the cooling of the baryons. But although the model can be parametrized in an even more sophisticated way, it offers one fundamental method of determining $\langle\kappa\rangle$, η and therefore H_0.

4.2.4 Results for the Semianalytic CDM Model

In the previous sections we saw how we can determine the Hubble constant based on a semianalytic model for the lensing mass distribution. Kochanek [30] uses four well-characterized time delay lenses to apply this model: PG 1115+080, SBS 1520+530, B1600+434 and HE 2149-2745. In a first step we determine the baryonic mass distribution using the photometric profile of the lensing galaxy and derive parameters which define the lens' geometry. The concentration c and the cold baryon fraction f_b remain as free variables in equation 4.42. The mean convergence $\langle\kappa\rangle$ and the logarithmic slope η can now be plotted depending on these free parameters. The two plots shown as examples for HE 2149-2745 in figure 21 and figure 22. We see that $\langle\kappa\rangle$ and η depend only weakly

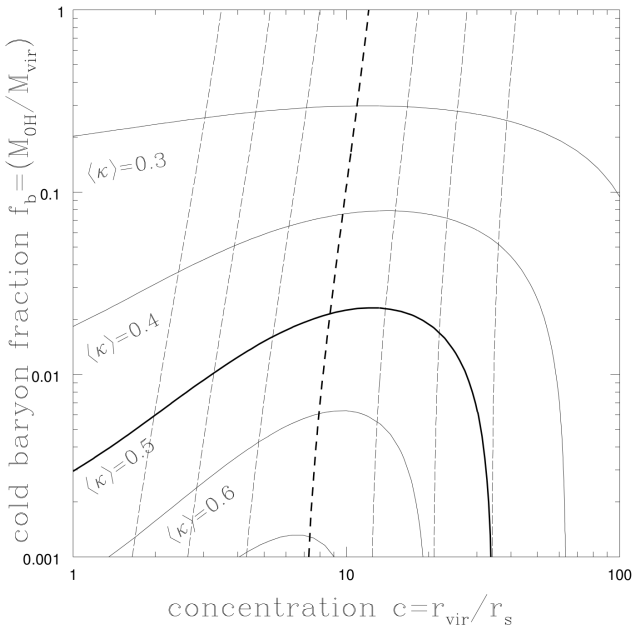

Figure 21: Average surface density $\langle\kappa\rangle$ of HE 2149-2745 as a function of the halo concentration $c = r_{vir}/r_s$ and the mass fraction of cold baryons in the visible galaxy $f_b = M_{0H}/M_{vir}$. The solid lines are contours of equal $\langle\kappa\rangle$ and the heavy solid contour indicates an isothermal model with $\langle\kappa\rangle = 0.5$. The heavy dashed line shows the most likely halo concentration and the light dashed contours show the 1, 2 and 3 σ ranges for the concentration distribution [30].

on the concentration. Therefore we can simplify the results by considering the concentration-probability-averaged values of $\langle\kappa\rangle$ and η as a function of f_b only. The results of this simplification are shown in figure 23 and 24 where the diagonally cross-hatched region shows the lower bound on f_b based on the local inventory of cold baryons. The horizontally cross-hatched region shows the upper bound on f_b, set by the global ratio of Ω_b/Ω_0 estimated from the CMB. The results for the four gravitational lenses are almost similar for a fixed cold baryon fraction. For baryon fractions similar to local accounting for cold baryons ($f_b \approx 0.02$) the convergence and the logarithmic slope are remarkably close to the isothermal values of $\langle\kappa\rangle = 0.5$ and $\eta = 2$. Whereas the CMB value for the cold baryon fraction suggests a lens model roughly in the middle of isothermal and a constant M/L model. Finally we can calculate the value of the Hubble constant according to equation 4.24. The coefficients for the single lenses are presented in table 1. In figure 25 we see that the four

Lens	A	B	C
PG 1115+080	92.3	4.6	0
SBS 1520+530	93.2	10.5	0
B 1600+434	103.9	20.6	0
HE 1149-2745	84.4	13.6	0

Table 1: Coefficients in units of km s^{-1}Mpc^{-1} [30].

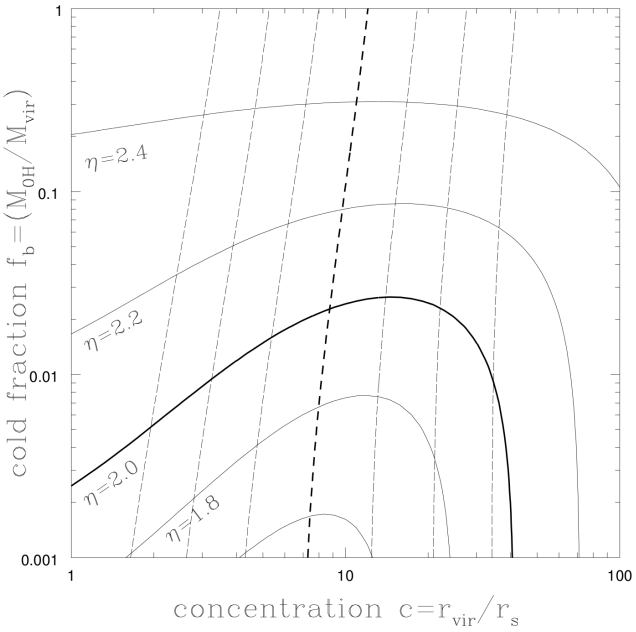

Figure 22: Average logarithmic slope ($\kappa \propto R^{1-\eta}$) in the annulus between the images of HE 2149-2745 as a function of the halo concentration $c = r_{vir}/r_s$ and the mass fraction of cold baryons in the visible galaxy $f_b = M_{0H}/M_{vir}$. The solid lines are contours of η and the heavy solid contour indicates an isothermal model with $\eta = 2$. The heavy dashed line shows the most likely halo concentration and the light dashed contours show the 1, 2 and 3 σ ranges for the concentration distribution [30].

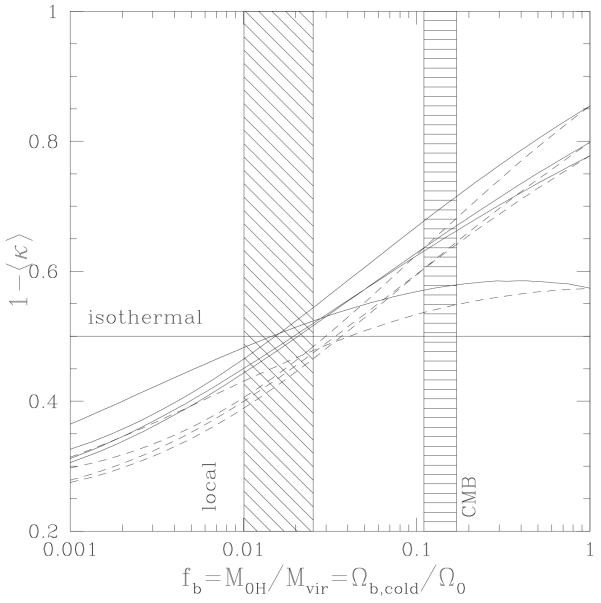

Figure 23: Concentration-averaged estimates for $1 - \langle\kappa\rangle$ as a function of f_b for the four mentioned gravitational lenses. The solid (dashed) curves represent the models with (without) adiabatic compression. The horizontal line marks the expected value for isothermal models [30].

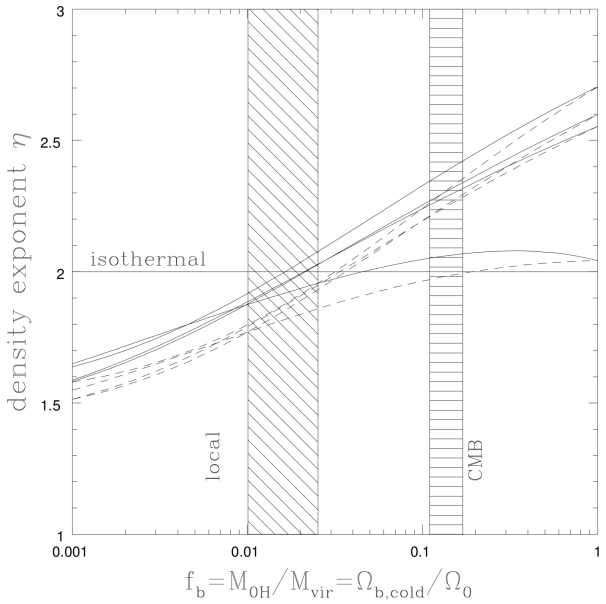

Figure 24: Concentration-averaged estimates for η as a function of f_b for the four mentioned gravitational lenses. The solid (dashed) curves represent the models with (without) adiabatic compression. The horizontal line marks the expected value for isothermal models [30].

lenses yield similar values of H_0 as a function of f_b. The final value of H_0 depends on the halo model: If the baryon density is restricted to agree with the local baryon density, equation 4.24 yields $H_0 = (52 \pm 6)$km s^{-1}Mpc^{-1} and if it is restricted to agree with the global baryon inventory, it yields $H_0 = (65 \pm 6)$km s^{-1}Mpc^{-1}.
Although the calculation of the Hubble constant can be complex in detail, we have seen the whole process of the determination and know that H_0 mainly depends on the mean convergence in the annulus $\langle\kappa\rangle$ and the logarithmic slope η, which can both be related to the cold baryon mass fraction f_b.

4.3 Statistical Assessment of Lens Model Dependences and their Impact on H_0

Time delays between lensed multiple images are a very elegant way to measure the Hubble constant. But in many cases, the accuracy of this method is limited by measurement errors or degeneracies of the lensing potential. Therefore it is convenient to use a statistical approach in order to limit the bounds of H_0. Even if the individual lenses do not supply enough information that allow detailed investigation of the mass distribution, a combination of many lenses can put tight constraints on the Hubble constant. This approach was realized by Saha [32] who combined 10 lensed quasar systems to constrain Hubble's parameter. But unfortunately this method suffers from selection effects: Obviously it is more likely to observe brighter quasars, but bright quasars are generally in denser environments such as groups and clusters. Generally spoken, we have to ensure that our lenses are randomly distributed but in most cases we can not be sure about this requirement. Another kind of statistical approach is presented by Oguri 2007 [33]. In contrast to Saha's method who firstly fits image positions of individual lens systems and combines them afterwards, Oguri apply the statistics to the lens parameters. This has the advantage that we can also include lens systems that have too few constraints to determine the lensing potential properly. Using analytic and numerical methods, this approach enables us to distinguish between image configurations which are sensitive to the detailed structure of the lens and image configurations which are stable. Sensitivity means, that even small variations in the potential lead to remarkable changes in the

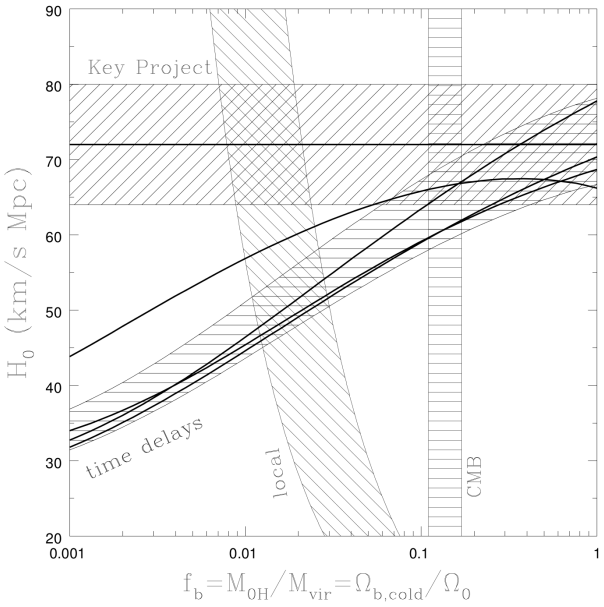

Figure 25: The Hubble constant as a function of f_b. The heavy curves show the results for the individual lenses. The shaded envelope bracketing the curves is the 95% confidence region for the combined lens sample. The vertical bands show the lower bound on f_b from local inventories, including its H_0 scaling, and the upper bound from the CMB. The horizontal band shows the estimate of $H_0 = (72 \pm 8)$km s^{-1}Mpc^{-1} by the HST Key Project [30].

observational parameters. This distinction is very helpful because it is almost impossible to extract an accurate value of H_0 from a very sensitive image configuration. This analysis can hence be used to select which lens systems are more suitable for further determinations of H_0.

4.3.1 Introducing Dimensionless Parameters

We want to describe the lensing properties based on dimensionless parameters and derive a distribution of time delays by adopting realistic lens models. We introduce a coordinate system with its origin in the centre of the lens and a source at the position $\vec{u} = (u_1, u_2)$. The image positions can be expressed by polar coordinates

$$\vec{x}_i = (x_i, y_i) = (r_i \cos\theta_i, r_i \sin\theta_i) \tag{4.43}$$

and the time delay between these images is

$$\Delta t_{ij} = \frac{1}{c}\frac{w_d w_s}{w_{ds}} \left(\frac{(\vec{x}_i - \vec{u})^2}{2} - \frac{(\vec{x}_j - \vec{u})^2}{2} - \psi(\vec{x}_i) + \psi(\vec{x}_j) \right) \tag{4.44}$$

which depends on parameters that are not directly observable. According to Witt et al. [34] a generalized isothermal potential $\psi(\vec{x})$ can be separated in the following way

$$\psi(\vec{x}) = rF(\theta) \tag{4.45}$$

where r is the radial coordinate and $F(\theta)$ is a function of θ. Using this result, the time delay can be expressed in a simplified form

$$\Delta t_{ij} = \frac{1}{2c}\frac{w_d w_s}{w_{ds}}(r_j^2 - r_i^2) \tag{4.46}$$

which depends only on the observable distance of the images from the centre of the lens. It is convenient to introduce the reduced time delay

$$\Xi = 2c\left|\frac{\Delta t_{ij}}{r_j^2 - r_i^2}\right|\frac{w_{ds}}{w_d w_s} = \left|\frac{(\vec{x}_i - \vec{u})^2 - (\vec{x}_j - \vec{u})^2 - 2\psi(\vec{x}_i) + 2\psi(\vec{x}_j)}{r_j^2 - r_i^2}\right| \tag{4.47}$$

which is unity if the lensing potential is isothermal but can deviate from 1 if the potential is perturbed e.g. by substructures or external shear. Using the results of Kochanek (equation 4.13), the reduced time delay can be expressed by $\Xi = 2(1 - \langle\kappa\rangle)$ to first order in $\Delta R/\langle R\rangle$. The reduced time delay measures the complexity of the lens system and indicates deviations from the simple isothermal mass distribution. As Ξ is a dimensionless quantity, we can directly compare systems of different reduced time delays regardless of the actual size of the lens. Another important dimensionless quantity of the lens system is the asymmetry of the images defined by

$$R_{ij} = \left|\frac{r_j - r_i}{r_j + r_i}\right|. \tag{4.48}$$

The asymmetry is close to zero if the images are roughly at the same distance from the lens centre while we find $R_{ij} \approx 1$ for very asymmetric configurations. The third parameter is the opening angle θ_{ij} of the images

$$\cos\theta_{ij} = \frac{\vec{x}_i \vec{x}_j}{r_i r_j} \tag{4.49}$$

which is close to zero for almost merging images and $\theta_{ij} \approx 180°$ for opposing images. The two quantities R_{ij} and θ_{ij} configure the lens geometry and can be observed if the centre of the lens galaxy is identifiable. This means that we do not have to assume any mass models in order to calculate these parameters. In a next step we want to analyse model dependences of the reduced time delay as a function of the image configuration parameters R_{ij} and θ_{ij}.

4.3.2 Modelling Realistic Lens Models Based on Various Potential Distributions

We want to study various lensed image pairs and therefore many different lensing potentials are generated by a Monte Carlo simulation. But before we can do this, we have to find a general and suitable model in order to cover all possible lensing effects. This is just a summary of the contributions and assumptions which are presented more detailed in [33].

Elliptical Galaxy: More than 80% of the quasars are lensed by elliptical galaxies and hence it is convenient to consider elliptical galaxies as primary lenses. We can write the associated convergence in the form

$$\kappa_G(\vec{x}) = \frac{\alpha}{2}\left[\frac{R_{Ein}}{r\sqrt{1 - \varepsilon\cos(2(\theta - \theta_e))}}\right]^{2-\alpha} \tag{4.50}$$

where R_{Ein} is the Einstein radius (equation 3.78), θ_e is the position angle of the ellipse and α defines the logarithmic slope of the density distribution. Note that this is connected to our previous notation by $\alpha = \eta - 1$ and $\alpha = 1$ corresponds to the standard isothermal mass distribution. The ellipticity e is related to the parameter ε by

$$\varepsilon = \frac{1 - (1 - e)^2}{1 + (1 - e)^2}. \tag{4.51}$$

The corresponding lensing potential is

$$\psi_G(\vec{x}) = \frac{1}{\alpha}{R_{Ein}}^{2-\alpha} r^\alpha G(\theta) \tag{4.52}$$

where $G(\theta)$ is a complex trigonometric function of the angle θ with the special case $G(\theta) = 1$ for vanishing ellipticity. Observations have indeed shown that elliptical galaxies have an almost isothermal mass distribution. Based on many previous works, Oguri adopts a Gaussian distribution $\alpha = 1 \pm 0.15$ "as a conservative distribution of the slope" and $e = 0.3 \pm 0.16$ for the ellipticity which is consistent with observations.

Multipole Terms: As we want to create realistic lensing potentials, we include multipole terms of the order $m = 3$ and $m = 4$ into the potential. The multipole expansion can be expressed by

$$\psi_M(\vec{x}) = \frac{1}{\alpha} {R_{Ein}}^{2-\alpha} r^\alpha \sum_m (1 - m^2) A_m \cos(\theta - \theta_m) \tag{4.53}$$

and has to be added to the elliptical lensing potential of equation 4.52.

External Perturbations: We also have to consider external perturbations in order to create lens environments. The external shear is modelled by

$$\psi_{E2}(\vec{x}) = -\frac{\gamma}{2} r^2 \cos(2(\theta - \theta_\gamma)) \tag{4.54}$$

and we adopt a lognormal distribution with median shear amplitude $\gamma = 0.05$ and dispersion 0.2dex which is consistent with N-body simulations [33]. In addition we include a third-order perturbation e.g. an external singular isothermal object described by the lensing potential

$$\psi_{E3}(\vec{x}) = \frac{\sigma}{4} \frac{r^3}{R_{Ein}} [\cos(\theta - \theta_\sigma) - \cos(3(\theta - \theta_\sigma))] \tag{4.55}$$

with a small misalignment θ_σ of the position angle and the amplitude σ which can generally be related to the shear by $\sigma \approx \gamma^2$.

Subhalos: Anomalous flux ratios observed in many gravitational lens systems indicate substructures of the lens. These substructures are mainly subhalos in the lensing galaxy and additionally we assume small halos along the line of sight. Each subhalo is modelled with a pseudo-Jaffe (truncated singular isothermal) profile and contributes to the total lensing potential by the term

$$\psi_{PJ,k}(\vec{x}) = b_k \left(r - \sqrt{r^2 + a_k^2} - \frac{a_k}{2} \ln \left| \frac{\sqrt{r^2 + a_k^2} - a_k}{\sqrt{r^2 + a_k^2} + a_k} \right| + a_k \ln r \right) \tag{4.56}$$

with the truncation radius a_k and the mass normalisation b_k. The subhalos are distributed randomly in the two dimensional lens plane and their total contribution is the sum over the individual potentials corrected for the convergence $\bar{\kappa}$ averaged over all subhalos

$$\psi_S(\vec{x}) = \sum_k \psi_{PJ,k}(\vec{x} - \vec{x}_{sub,k}) - \frac{1}{2} r^2 \bar{\kappa}. \tag{4.57}$$

4.3.3 Simulation of Lensing Potentials and Image Pairs

In a next step Oguri combines the presented lensing potential contributions. A Monte Carlo simulation creates 10000 different lensing potentials and places randomly sources in the source plane. The public software Lensmodel solves the lens equation, determines the image positions and computes the time delays. Now we have a catalogue of various gravitational lenses with corresponding image configurations which are very close to realistic ones. Based on the reduced time delay, we can now investigate to what extend these randomly created lenses deviate from a simple isothermal potential. In order to trace back the individual influences, it is convenient to study the contributions to the lensing potential separately.

4.3.4 Contributions from the Lensing Potentials

We assume an isothermal ($\alpha = 1$) elliptical lensing potential with multipole terms ($\psi_G + \psi_M$) as a basis. Now we add the potentials separately and calculate the deviations from $\Xi = 1$ which is a quantification of the nonisothermality and subsequently of the lens model's complexity. The overall aim is to investigate under which conditions the time delay Δt_{ij} is stable against small perturbations in the lens model. The distinction of stable and sensitive lenses can only be based on observational quantities and therefore it is convenient to plot the reduced time delay as a function of the asymmetry R_{ij} and the opening angle θ_{ij}. The results of this analysis are shown in figure 26 and can be summarized as follows:

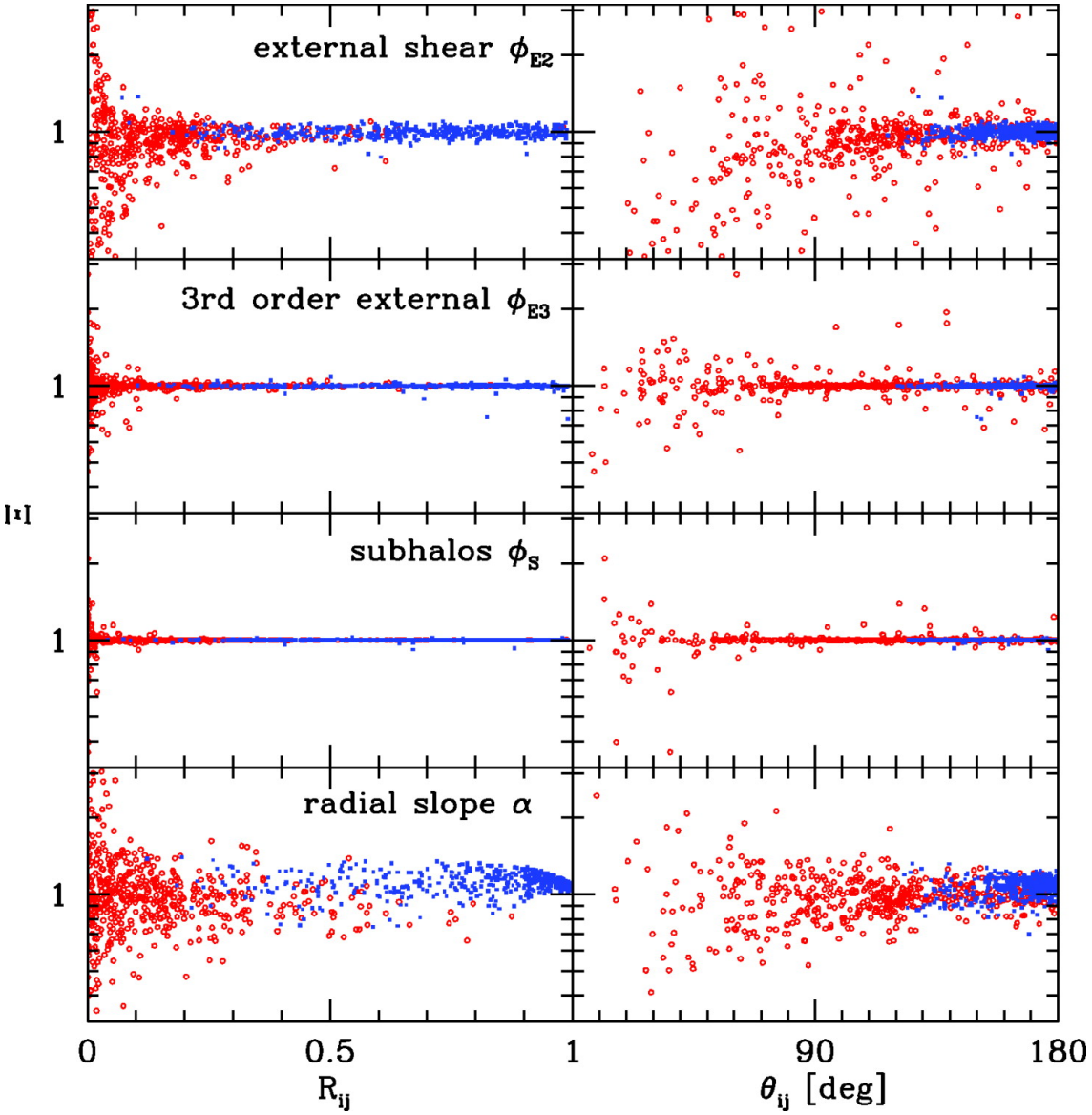

Figure 26: Dependence of the reduced time delay Ξ on several lensing potentials as a function of asymmetry R_{ij} (left) and opening angle θ_{ij} (right). In each panel, reduced time delays of 500 double lenses (blue squares) and 500 quadruple lenses (red circles) obtained by Monte Carlo simulations are plotted. From top to bottom, we consider the external shear ψ_{E2} (equation 4.54), third-order external perturbations ψ_{E3} (equation 4.55), subhalos ψ_S (equation 4.57) and nonisothermality $\alpha \neq 1$ in the primary lens model ψ_G (equation 4.52). For each panel we focus on one modification and ignore the other perturbations, thus the effect of each type of perturbation can be measured by the deviation from $\Xi = 1$ [33].

- The **External shear** creates a scatter of Ξ around one as expected from the analytic examination but it preferentially produces image pairs with $\Xi < 1$ which corresponds to a steeper

than isothermal profile. We can observe a remarkable scatter of quadruple lenses for small opening angles.

- The **third-order external perturbations** create almost the same effects as the external shear but the amplitudes of the scatter are smaller.
- In the same way the **subhalos** have a small influence on the reduced time delay and the scatter is marginal except for quadruple lenses with a small opening angle which create relatively strong deviations.
- The **radial slope** as a quantification of the nonisothermality has a strong impact on Ξ. The scatter is distinct for double and quadruple lenses and it is less dependent on the image configuration than the other contributions.
- Generally we can see that the **asymmetry** has remarkable influence only for image positions that are almost equidistant from the lens. In all four cases the symmetric images are very sensitive for perturbations and therefore cause a large scatter.
- The **opening angle** has a strong influence on the stability of the reduced time delay and even $\theta_{ij} \approx 90°$ causes a significant scatter. The most stable image configurations are opposite images ($\theta_{ij} = 180°$).
- The stability of **double and quadruple lenses** shows almost the same dependence on the asymmetry R_{ij} but the scatter of the opening angle θ_{ij} is clearly dominated by quadruple lenses.

This analysis enables us to check, which image configurations are less dependent on the exact lensing potentials. We can conclude, that double lenses with asymmetric image configuration and almost opposite images have the least scatter and are therefore most suitable for determining the Hubble constant. Although double lenses effect less scatter, quadruple lenses provide more information about the lensing potential. Hence the number of images can not be used as a reliable definition for valuable image configurations.
These results are an enormous help for further studies because on the one hand we know how stable certain image configurations are regarding small variations in the lens model and on the other hand we have discovered the relative strengths of the perturbing components.

5 Error Propagation and Dependence on the Mass Model

In the last sections we introduced different methods and ways of determining the Hubble constant. All methods have in common, that they are based on observable quantities. In this chapter we want to analyse the influence of the individual parameters. Especially in cosmology, the errors are relatively large and therefore it is important to know, which parameters have a significant influence and which parameters have a negligible effect. Based on this analysis we can name quantities which should be measured more precisely in order to receive proper values and reliable errors for Hubble's parameter. As we will see, the accuracy of the the Hubble constant's determination and its error does not only depend on the measured quantities but also on the mass model and the complexity of the lensing potential. Hence we also assume different mass distributions for one and the same set of observed parameters.

5.1 Generalised Lens System

We are targeting an analysis of the quadruple lens system B1608+656 but before we study this special case, we want to analyse a generalised lens system in order to understand the qualitative behaviour and error propagation.

5.1.1 Assumptions for the Lens System

Let us assume the following settings: The model lensing galaxy is well described by a singular isothermal ellipsoid (SIE) with external shear. This model can be analysed analytically but is still complex enough to see variations from simpler models. In this first part of the analysis we are interested in two effects: First we want to know the influence of each single parameter and we want to see whether the errors are amplified or damped. Second we want to analyse the dependence on the mass model and therefore we take the SIE with external shear as a reference, apply simplified mass models and determine the changes.
First of all we have to set up and specify the lensing potential and the corresponding deflection angle. For the analysis it is convenient to introduce the dimensionless parameter

$$\kappa_0 = 4\pi \left(\frac{\sigma}{c}\right)^2 \frac{w_{ds}}{w_s} \tag{5.1}$$

in order to simplify the following equations. The lensing potential of a SIE is given by

$$\psi_e(\theta_1, \theta_2) = \kappa_0 \sqrt{(1-\epsilon)\theta_1^2 + (1+\epsilon)\theta_2^2} \tag{5.2}$$

with the ellipticity ϵ and the angular positions θ_1 and θ_2 of the lensed image. The associated deflection angle is

$$\vec{\alpha}_e = \vec{\nabla}\psi_e(\theta_1, \theta_2) = \kappa_0 \frac{1}{\sqrt{(1-\epsilon)\theta_1^2 + (1+\epsilon)\theta_2^2}} \begin{pmatrix} (1-\epsilon)\theta_1 \\ (1+\epsilon)\theta_2 \end{pmatrix}. \tag{5.3}$$

According to equation 3.125 the shear potential can be expressed by

$$\psi_s(\theta_1, \theta_2) = \frac{\gamma_1}{2}(\theta_1^2 - \theta_2^2) + \gamma_2\theta_1\theta_2 \tag{5.4}$$

with the shear amplitudes γ_1 and γ_2. The corresponding deflection angle yields

$$\vec{\alpha}_s = \vec{\nabla}\psi_s(\theta_1, \theta_2) = \begin{pmatrix} \gamma_1\theta_1 + \gamma_2\theta_2 \\ -\gamma_1\theta_2 + \gamma_2\theta_1 \end{pmatrix} \tag{5.5}$$

and the lens equation turns into

$$\vec{\beta} = \vec{\theta} - \vec{\alpha} = \vec{\theta} - (\vec{\alpha}_e + \vec{\alpha}_s). \tag{5.6}$$

As we want to study a realistic lensing system, we have to calculate the image positions and time delay depending on the lens geometry. Therefore we set the lens' parameters to $z_s = 1.5$, $z_d = 0.5$, $\sigma = 260\text{km s}^{-1}$, $\epsilon = \gamma_1 = \gamma_2 = 0.15$, $\Omega_m = 0.27$ and $\Omega_\Lambda = 0.73$. These parameters are chosen close to existing lensing systems (compare table 4) and the lensing potentials are shown in figure 27, 28 and 29. In order to obtain the image positions, we have to solve the system of equations

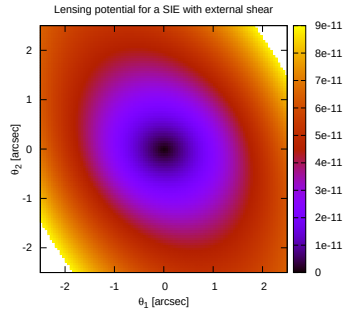

Figure 27: SIE with external shear as initial lensing potential.

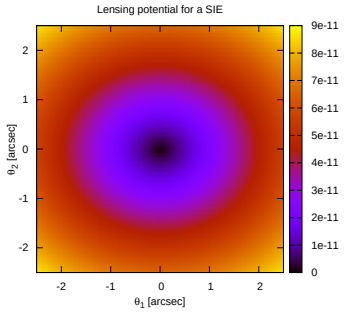

Figure 28: First simplification of the lensing potential (SIE).

$$\beta_1 = \theta_1 - \frac{\kappa_0(1-\epsilon)\theta_1}{\sqrt{(1-\epsilon)\theta_1^2 + (1+\epsilon)\theta_2^2}} - \gamma_1\theta_1 - \gamma_2\theta_2, \tag{5.7}$$

$$\beta_2 = \theta_2 - \frac{\kappa_0(1+\epsilon)\theta_2}{\sqrt{(1-\epsilon)\theta_1^2 + (1+\epsilon)\theta_2^2}} + \gamma_1\theta_2 - \gamma_2\theta_1. \tag{5.8}$$

We place the source at $\beta_1 = 0.5''$,$\beta_2 = 1''$ and determine the image positions numerically with Maple. The image positions are listed in table 2 and can be seen in figure 30. Oguri's analysis

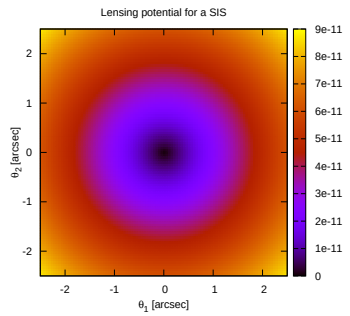

Figure 29: Second simplification of the lensing potential (SIS).

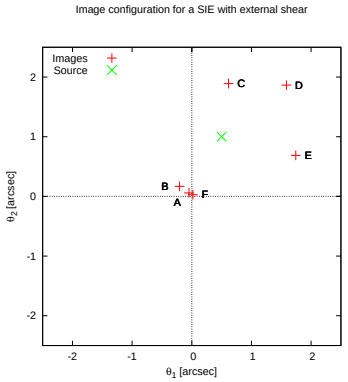

Figure 30: Source and image positions for a SIE with external shear.

suggests the choice of image A and D for further analysis because they are located asymmetric and almost collinear with the lens. But unfortunately these images are too stable and we might not see any significant deviations. Hence we choose image B and C where we can investigate more

Image	θ_1	θ_2
A	$-0.047''$	$0.058''$
B	$-0.206''$	$0.168''$
C	$0.616''$	$1.892''$
D	$1.586''$	$1.866''$
E	$1.743''$	$0.689''$
F	$0.019''$	$0.028''$

Table 2: Image positions for a SIE with external shear and a source located at $\vec{\beta} = (0.5'', 1'')$.

interesting effects. In a next step we have to calculate the time delay for the selected images

$$\begin{aligned}\Delta t_i &= \frac{1}{c}\frac{w_s w_d}{w_{ds}}\left(\frac{\vec{\alpha}(\theta_{1i},\theta_{2i})^2}{2} - \psi(\theta_{1i},\theta_{2i})\right) \\ &= \frac{1}{c}\frac{w_s w_d}{w_{ds}}\left(\frac{1}{2}\left[\vec{\alpha}_e(\theta_{1i},\theta_{2i}) + \vec{\alpha}_s(\theta_{1i},\theta_{2i})\right]^2 - \left[\psi_e(\theta_{1i},\theta_{2i}) + \psi_s(\theta_{1i},\theta_{2i})\right]\right). \end{aligned} \tag{5.9}$$

Furthermore we have to keep in mind that the comoving distances are given by

$$w_{ij} = -\int_{a_i}^{a_j} \frac{\mathrm{d}a}{a}\frac{c}{H_0}\left[a(t)^{-4}\Omega_r + a(t)^{-3}\Omega_m + a(t)^{-2}\Omega_k + \Omega_\Lambda\right]^{-1/2} \tag{5.10}$$

which yields the dependence on Hubble's parameter. As measurements have shown, the radiation and the curvature term can be neglected and the integral simplifies to

$$w_{ij} = -\frac{c}{H_0}\int_{a_i}^{a_j} \frac{\mathrm{d}a}{\sqrt{a^{-1}\Omega_m + a^2\Omega_\Lambda}} \tag{5.11}$$

which has to be calculated numerically nevertheless. For further simplification we define the integral

$$W_{ds} = \int_{a_s}^{a_d} \frac{\mathrm{d}a}{\sqrt{a^{-1}\Omega_m + a^2\Omega_\Lambda}} \tag{5.12}$$

and W_s and W_d correspondingly and we recall that the scale function is related to the redshift by $a_s = (1+z_s)^{-1}$. Inserting the definitions of the potentials, deflections angles and comoving distances we obtain

$$\begin{aligned} H_0\Delta t_i = &\frac{W_s W_d}{W_{ds}}\left[\frac{\kappa_0^2}{2}\frac{(1-\epsilon)^2\theta_{1i}^2 + (1+\epsilon)^2\theta_{2i}^2}{(1-\epsilon)\theta_{1i}^2 + (1+\epsilon)\theta_{2i}^2}\right] \\ &+ \frac{W_s W_d}{W_{ds}}\left[\frac{1}{2}(\gamma_1\theta_{1i} + \gamma_2\theta_{2i})^2 + \frac{1}{2}(\gamma_2\theta_{1i} - \gamma_1\theta_{2i})^2\right] \\ &+ \frac{W_s W_d}{W_{ds}}\left[\kappa_0\frac{(1-\epsilon)\theta_{1i}(\gamma_1\theta_{1i} + \gamma_2\theta_{2i}) + (1+\epsilon)\theta_{2i}(\gamma_2\theta_{1i} - \gamma_1\theta_{2i})}{\sqrt{(1-\epsilon)\theta_{1i}^2 + (1+\epsilon)\theta_{2i}^2}}\right] \\ &+ \frac{W_s W_d}{W_{ds}}\left[\kappa_0\sqrt{(1-\epsilon)\theta_{1i}^2 + (1+\epsilon)\theta_{2i}^2} - \frac{\gamma_1}{2}(\theta_{1i}^2 - \theta_{2i}^2) - \gamma_2\theta_{1i}\theta_{2i}\right]. \end{aligned} \tag{5.13}$$

We can calculate the time delay $\Delta t_{BC} = \Delta t_C - \Delta t_B$ up to a factor of H_0 and obtain the whole set of lensing parameters (table 3). We set each relative error to 10% with a Gaussian distribution. As we will see later on, this might be exaggerated for certain quantities but nevertheless this choice is convenient for a better comparability of the individual influences. Solving equation 5.13 for H_0 yields an expression for the Hubble constant that depends on 13 parameters

$$H_0 = H_0(\Delta t_{BC}, z_d, z_s, \sigma, \theta_{1B}, \theta_{2B}, \theta_{1C}, \theta_{2C}, \epsilon, \gamma_1, \gamma_2, \Omega_m, \Omega_\Lambda). \tag{5.14}$$

The time delay still depends on Hubble's parameter but as we are interested in the relative fraction of true and disturbed value $H_0(\vec{x} + \delta\vec{x})/H_0(\vec{x})$, this dependence cancels out.

Parameter	Symbol	Value x_0	Absolute Error Δx	Relative Error
Time difference	Δt_{BC}	$3.32 \cdot 10^{-11} H_0^{-1}$	$3.32 \cdot 10^{-12} H_0^{-1}$	10%
Redshift lens	z_d	0.5	0.05	10%
Redshift source	z_s	1.5	0.15	10%
Dispersion velocity	σ	260km s^{-1}	26km s^{-1}	10%
Position image B 1	θ_{1B}	$-0.206''$	$0.021''$	10%
Position image B 2	θ_{2B}	$0.168''$	$0.017''$	10%
Position image C 1	θ_{1C}	$0.616''$	$0.062''$	10%
Position image C 2	θ_{2C}	$1.892''$	$0.189''$	10%
Ellipticity	ϵ	0.15	0.015	10%
Shear amplitude 1	γ_1	0.15	0.015	10%
Shear amplitude 2	γ_2	0.15	0.015	10%
Matter density	Ω_m	0.27	0.027	10%
Dark energy density	Ω_Λ	0.73	0.073	10%

Table 3: Parameters of a model lens system. The values are close to real parameters in order to ensure an authentic model.

5.1.2 Numerical Procedure

In this chapter we want to discuss briefly the used programmes. The first programme analyses the influence of each parameter individually: As input variables we have 13 parameters x_i and their relative errors of 10% from where we can derive the absolute errors $\Delta x_i = \sigma_i$. First we calculate the "true" H_0 in order to be able to compare the disturbed results. Then we vary one parameter in the interval $[x_i - 5\sigma_i, x_i + 5\sigma_i]$ and keep the remaining values fixed. For each step in the interval we calculate the corresponding a priori probability and the disturbed value for Hubble's parameter which is afterwards normalised by the true H_0. Proceeding in the same way for the remaining 12 parameters, we receive probability distributions that relate the deviation of the original value to a probability.
The second programme analyses the model dependence: First, we calculate H_0 with the exact values as a reference and then use a Monte Carlo simulation to study the error propagation. The Hubble constant is calculated 1 million times with randomly created parameters. The random function creates a Gaussian distribution which generates independent values for the 13 input parameters according to their particular σ_i. These values for the Hubble constant are divided by the true value, stored in a histogram and normalized by the number of calculations. This procedure is executed for the SIE with external shear, for the SIE ($\gamma_1 = 0, \gamma_2 = 0$) and for the SIS ($\gamma_1 = 0, \gamma_2 = 0, \epsilon = 0$) so that we can compare the corresponding histograms and the model dependence.

5.1.3 Results of the Error Propagation

Here we want to present and discuss the results of the first analysis. The parameters are divided in 5 categories for a better overview of the plots. Each plot contains additionally a Gauss function with $\mu = 1$ and $\sigma = 0.1$ which represents the case of linear error propagation. If the calculated probability distribution is narrower than the Gauss function, the error is damped and if it is broader than the Gauss function the error is amplified.

- **Cosmological parameters:** The corresponding probability distributions are shown in figure 31. The parameters Ω_Λ and Ω_m enter only the integral in equation 5.12 and affect the value of H_0 little. Both errors are damped and both probability distributions are slightly asymmetric: Ω_Λ prefers lower values of Hubble's parameter whereas Ω_m prefers higher values.

- **Redshifts:** The corresponding probability distributions are displayed in figure 32 and the lens' redshift z_d contributes almost linearly. The probability distribution of the source's redshift z_s is asymmetric, preferring smaller values of H_0. Hence we can conclude that

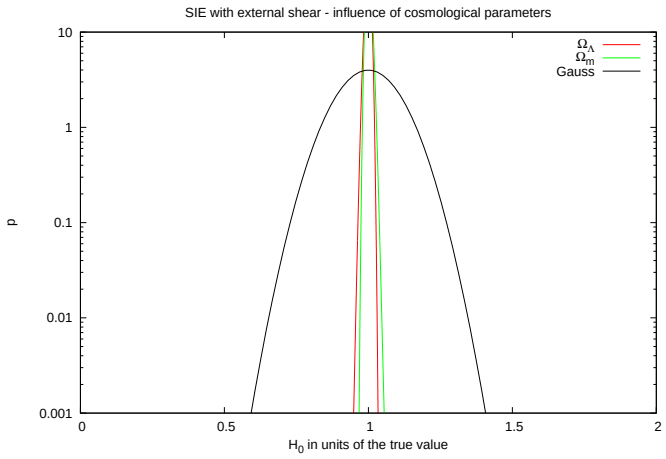

Figure 31: Error propagation for the cosmological parameters with a relative error of 10%.

uncertainties in z_s rather decrease the values of H_0 for this lens system.

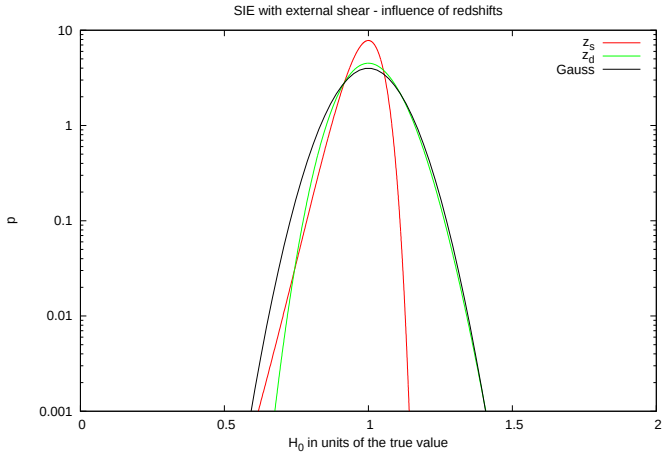

Figure 32: Error propagation for the redshifts with a relative error of 10%.

- **Velocity dispersion and time difference:** The corresponding probability distributions are shown in figure 33. As the time difference Δt_{BC} enters inversely, the error propagates almost linearly and the probability distribution is just shifted a little bit to higher values of H_0, compared to the standard Gaussian. The velocity dispersion σ describes mainly the dynamics of the lens galaxy and therefore its error is remarkably (mind the logarithmic scale) amplified.

- **Image positions:** The corresponding probability distributions are shown in figure 34. They are quite symmetric and the errors of the parameters θ_{1B}, θ_{2B} and θ_{1C} are damped for this lens system. Therefore we can conclude, that small variations in these quantities do not effect Hubble's parameter remarkably. Only the angular position θ_{2C} obeys an almost linear error propagation.

- **Ellipticity and shear:** The corresponding probability distributions are shown in figure 35. Variations of the exact values for ellipticity ϵ and shear γ_1, γ_2 have only very little influence on Hubble's parameter. The errors are damped strongly and the distributions are fairly symmetric. Hence, the relative errors of 10% have no significant influence on this lens system.

We have to keep in mind, that these results are derived for one specific lens system and can not easily be generalised to other systems. Nevertheless we have seen the qualitative error propaga-

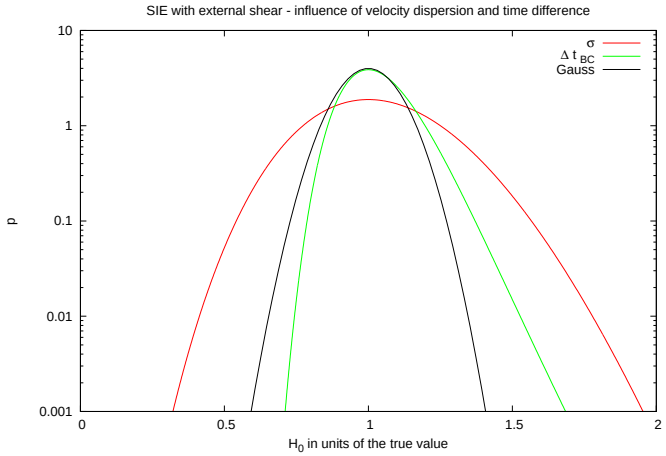

Figure 33: Error propagation for the velocity dispersion and time difference with a relative error of 10%.

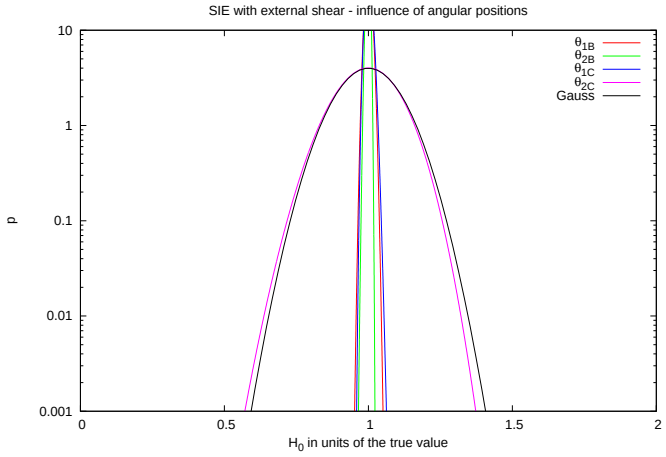

Figure 34: Error propagation for the image positions with a relative error of 10%.

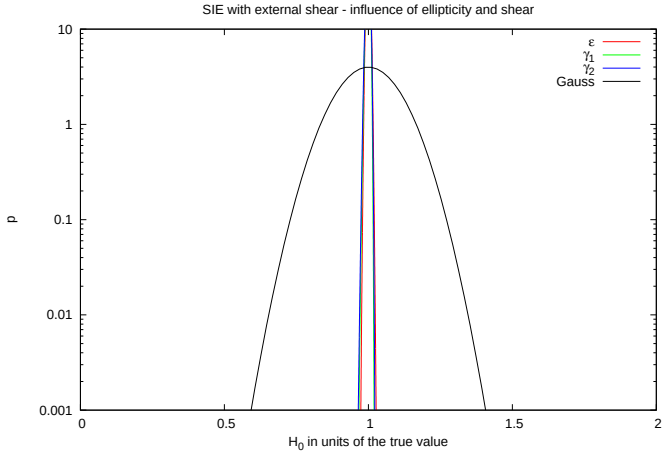

Figure 35: Error propagation for the asymmetry parameters with a relative error of 10%.

tion and investigated several remarkable effects: The errors of the time difference and velocity dispersion are amplified most strongly, whereas image positions, asymmetry parameters and the cosmological model do not effect Hubble's parameter significantly. The redshifts and therefore the cosmological distances are very important for an exact measurement of H_0. The redshifts' probability distributions are asymmetric, preferring smaller (z_s) or larger (z_d) values of the Hubble constant.

5.1.4 Results of the Mass Model Dependence

We now understand the individual parameters' influence on H_0 but moreover we have to control the influence of a wrong or too simple mass model. Therefore we assume the lens system to be exactly described by a SIE with external shear and analyse the consequences of a simplified mass model as described in the numerical procedure. The result of this analysis can be seen in figure 36. The probability distributions can be described remarkably well by a Gaussian: For the SIE

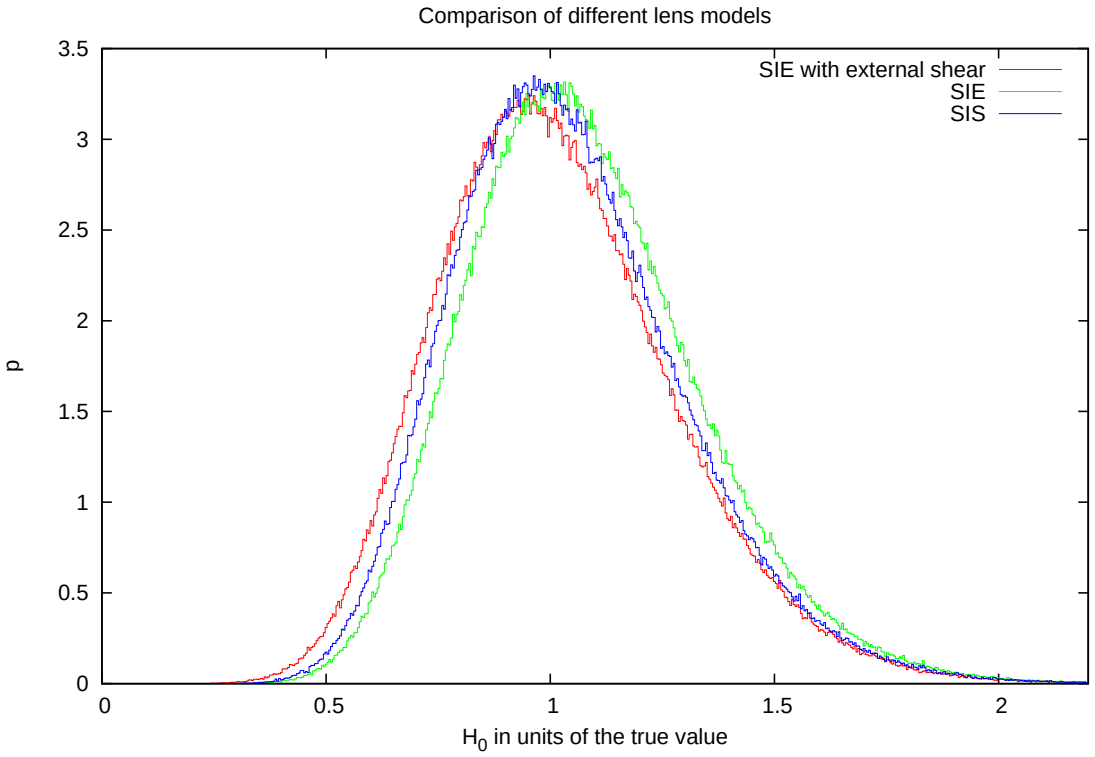

Figure 36: Comparison of a SIE with external shear and its simplifications. For each individual parameter we assume a Gaussian distribution with a relative error of 10% and use a Monte Carlo simulation with 1 million calculations for each model.

with external shear we find $\mu = 0.99$ and $\sigma = 0.25$. For the SIE the fit generates $\mu = 1.04$ and $\sigma = 0.24$ and for the SIS we receive $\mu = 1.01$ and $\sigma = 0.23$ with fit accuracies of less than 1%. The first interesting outcome is that simplifications do not always have a negative impact on the result. If we neglect the shear of the SIE, the programme yields values for Hubble's parameter that are about 4% higher than the true value. But if we simplify this SIE even further to a SIS, the most probable value of H_0 is just 1% above the true value. Furthermore we discover that simpler and more symmetric lens models create slightly narrower probability distributions and therefore are apparently less sensitive to errors. Summing up we can conclude that relative parameter errors of 10% lead to a relative error for the Hubble constant of $> 20\%$ whereas the uncertainties due to a wrong mass model yield deviations of $< 5\%$. But nevertheless we have to clarify whether real measurement errors lead to the same conclusion.

5.2 Analysis of the Lens System B1608+656

We want to specialise this general analysis to a specific lens model: B1608+656 is a quadruple gravitational lens with a radio galaxy's nucleus as a source and two galaxies acting as a lens. The image configuration is shown in figure 37. We are interested in the error propagation based on

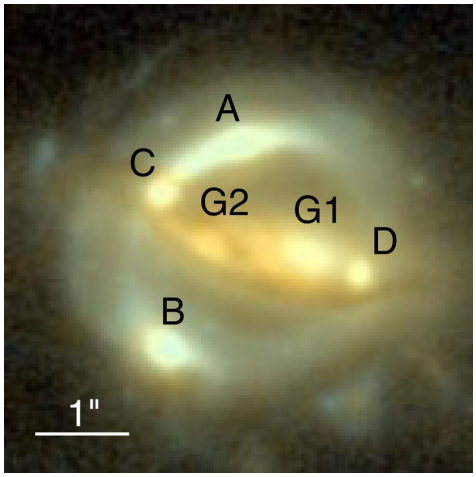

Figure 37: Observation of B1608+656 containing the galaxies G1 and G2 and the four images A, B, C and D [35].

realistic measurements and the dependence on the lens model. Furthermore we want to point out the most important parameters for the lens model which should be measured more precisely in order to constrain the error margins of Hubble's parameter and to provide guidance for further studies. Finally we determine the Hubble constant based on a given lens model with the help of the Monte Carlo simulation.

5.2.1 Assumptions for the Lens System

Although Keeton and Kochanek state "that B1608+656 requires a non-trivial lens model" [36], we use the ansatz by Myers et al. [37] and model the lens with a non singular isothermal ellipsoid. The lensing potential for this model can be expressed by

$$\psi = \kappa_0 \sqrt{\theta_c^2 + (1-\epsilon)\theta_a^2 + \theta_b^2} \tag{5.15}$$

with the core radius θ_c and the positions θ_a, θ_b that are defined in a coordinate system which is perpendicular to the ellipse's major and minor semi-axes. We have to relate these coordinates to the coordinates θ_1, θ_2 that are defined in a coordinate system with its axis pointing from west to east and south to north. Therefore we have to apply a rotation by the position angle φ

$$\begin{pmatrix} \theta_a \\ \theta_b \end{pmatrix} = \begin{pmatrix} \cos\varphi & -\sin\varphi \\ \sin\varphi & \cos\varphi \end{pmatrix} \begin{pmatrix} \theta_1 \\ \theta_2 \end{pmatrix} = \begin{pmatrix} \theta_1\cos\varphi - \theta_2\sin\varphi \\ \theta_1\sin\varphi + \theta_2\cos\varphi \end{pmatrix} \tag{5.16}$$

and the potential turns into

$$\psi = \kappa_0 \sqrt{\theta_c^2 + (1-\epsilon)(\theta_1\cos\varphi - \theta_2\sin\varphi)^2 + (\theta_1\sin\varphi + \theta_2\cos\varphi)^2}. \tag{5.17}$$

The deflection angle yields

$$\begin{aligned} \vec{\alpha} = \vec{\nabla}\psi = & \frac{\kappa_0}{\sqrt{\theta_c^2 + (1-\epsilon)(\theta_1\cos\varphi - \theta_2\sin\varphi)^2 + (\theta_1\sin\varphi + \theta_2\cos\varphi)^2}} \\ & \cdot \begin{pmatrix} (1-\epsilon)(\theta_1\cos\varphi - \theta_2\sin\varphi)\cos\varphi + (\theta_1\sin\varphi + \theta_2\cos\varphi)\sin\varphi \\ -(1-\epsilon)(\theta_1\cos\varphi - \theta_2\sin\varphi)\sin\varphi + (\theta_1\sin\varphi + \theta_2\cos\varphi)\cos\varphi \end{pmatrix} \end{aligned} \tag{5.18}$$

and the time delay can be expresses by

$$\Delta t_i = \frac{W_s W_d}{H_0 W_{ds}} \left(\frac{\vec{\alpha}(\theta_{1i}, \theta_{2i})^2}{2} - \psi(\theta_{1i}, \theta_{2i}) \right) \tag{5.19}$$

which can be solved for Hubble's parameter. The observed parameters and corresponding errors are listed in table 4. These values are mainly based on a paper by Myers et al. [37] and further

Parameter	Symbol	Value x_0	Absolute Error Δx	Relative Error
Time difference	Δt_{12}	36d	7d	19.4%
Redshift lens	z_d	0.6304	0.00063	0.1%
Redshift source	z_s	1.41	0.14	10%
Dispersion velocity	σ	311.7km s^{-1}	15km s^{-1}	4.8%
Position image B 1	θ_{1C}	$1.07''$	$0.0045''$	0.4%
Position image B 2	θ_{2C}	$-0.96''$	$0.0046''$	0.5%
Position image C 1	θ_{1D}	$1.08''$	$0.0045''$	0.4%
Position image C 2	θ_{2D}	$0.54''$	$0.0049''$	0.9%
Core radius	θ_c	$0.48''$	$0.10''$	21%
Ellipticity	ϵ	0.96	0.05	5%
Position angle	φ	67.0°	1.3°	2%
Matter density	Ω_m	0.27	0.02	7.4%
Dark energy density	Ω_Λ	0.73	0.02	2.7%

Table 4: Observable parameters for the quadruple lens system B1608+656

information:

- Time difference: The value and error are listed in [38]. We choose the images B and C for further analysis because they have the smallest time delay error.
- Redshift lens: Fassnacht et al. [38] provide the value and the relative error is chosen according to the high precision of the measurement.
- Redshift source: The value is provided by Myers et al. and the error has to be large because generally it is difficult to receive a satisfactory spectrum.
- Velocity dispersion: The values are listed by Myers et al. and the error is adopted from [33].
- Angular positions: Myers et al. provide image positions with the corresponding errors.
- Core radius: Given by Myers et al.
- Ellipticity: Myers et al. provide value and error. During the calculation we require $\epsilon \leq 0.999$.
- Position Angle: Myers et al. set this value as the angle between the major axis and the θ_1-axis.
- Critical densities: Schneider [14] provides a table with the cosmological parameters and corresponding errors.

5.2.2 Numerical Procedure

The two programmes work basically in the same way as described above but instead of using a relative error of 10%, we choose the errors according to table 4. The simplifications in the second part of the analysis are as follows: According to Myers et al. the non singular isothermal ellipsoid is the best model and we simplify it to a SIE ($\theta_c = 0$) and a SIS ($\theta_c = 0$, $\epsilon = 0 \Rightarrow \varphi$ is meaningless and can be set to zero).

5.2.3 Results of the Error Propagation

Since a qualitative analysis of the error propagation was already given above, we now focus on the new results and effects due to the real errors. The plots contain Gauss distributions ($\mu = 1$ and $\sigma = 0.1$) as a reference point.

- **Cosmological parameters:** The error propagation is damped for both parameters which underlines the statement that the determination of the Hubble constant by gravitational lensing depends only little on the cosmological model.

- **Redshifts:** The lens' redshift can be measured very precisely and therefore its error is negligible (figure 38). The error of the source's redshift propagates almost linearly, preferring higher values for the Hubble constant.

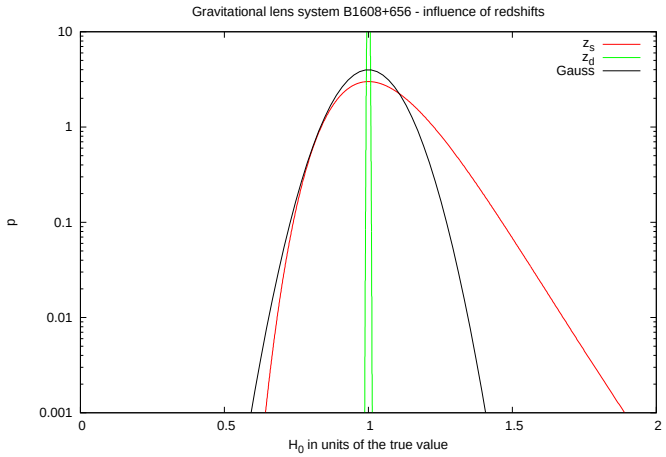

Figure 38: Error propagation for the redshifts.

- **Velocity dispersion and time difference:** The corresponding probability distributions are shown in figure 39. The error of the time delay is quite large and causes strong deviations to higher values of H_0. The probability distribution of the velocity dispersion is very asymmetric. It declines dramatically at about 1.05 and hence we can conclude that uncertainties in σ lead to smaller values of H_0 for this lens system.

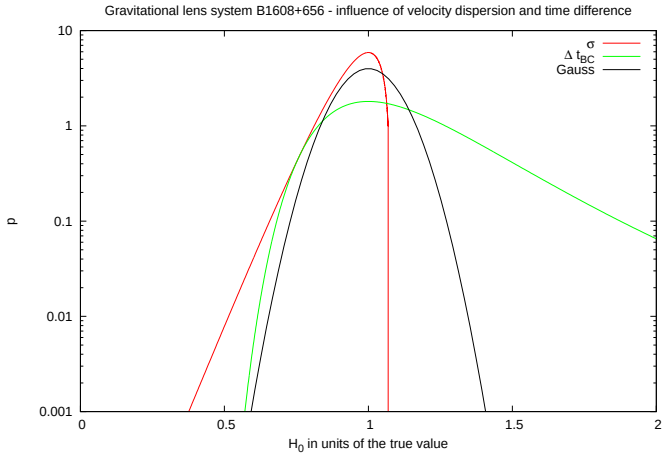

Figure 39: Error propagation for the velocity dispersion and time difference.

- **Image positions:** The angular positions of the images can be measured very precisely and their errors are negligible.

- **Core radius, ellipticity and position angle:** All three parameters have a huge influence on the measurement and their probability distributions can be seen in figure 40. Although the ellipticity has only small relative errors, the corresponding distribution function is very broad and asymmetric. There is a cut off point at about 1.4 which indicates the limiting ellipticity $\epsilon = 0.999$. Uncertainties in the position angle can not create values above the true one because the probability distribution declines at 1. The core radius has a significant influence and prefers higher values for Hubble's parameter.

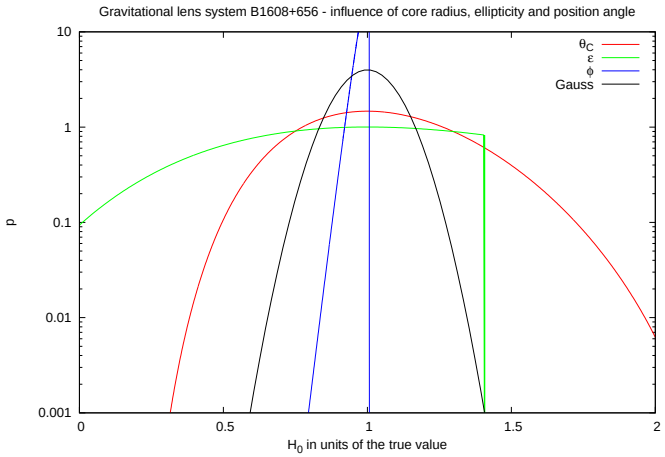

Figure 40: Error propagation for core radius, ellipticity and position angle.

This analysis has outlined very important information regarding the required accuracy of the model's parameters: Image positions, cosmological model and lens' redshift have a satisfying precision. The error of the Hubble constant is thereafter dominated by a few parameters: time delay, velocity dispersion, source's redshift, core radius, ellipticity and position angle. In order to obtain better estimates and smaller error margins for H_0 it is important to determine these parameters with higher accuracy.

5.2.4 Results of the Mass Model Dependence

We want to analyse the model dependence of the lens system B1608+656 in the same way as above but with the real errors. The result of the Monte Carlo simulation can be seen in figure 41. We fit a Gaussian function to these probability distributions and the values for the median and standard deviation are listed in table 5. We can again observe the effect that simplifications

Mass model	median μ	standard deviation σ
Non singular isothermal ellipsoid	48.3 km s^{-1}Mpc^{-1}	26.7 km s^{-1}Mpc^{-1}
Singular isothermal ellipsoid	108.4 km s^{-1}Mpc^{-1}	46.5 km s^{-1}Mpc^{-1}
Singular isothermal sphere	63.5 km s^{-1}Mpc^{-1}	9.1 km s^{-1}Mpc^{-1}

Table 5: Fit parameters for different lens models

of the model do not always shift the median in the same direction: The simplification from a non SIE to a SIE increases, the simplification from a non SIE to a SIS decreases the value. The SIS neglects 3 values that have a strong influence on the Hubble constant's error and therefore is the narrowest distribution. If we neglect the core radius, the probability distribution of the SIE is very broad which can be seen as an evidence for an unstable lens configuration. Moreover the SIE's shape slightly deviates from a Gauss function which might be caused by the very asymmetric error propagation for φ and ϵ.
The medians of the individual distributions are spread over a wide range whereas the standard deviations are comparatively small. Hence this analysis clearly outlines that the choice of a proper

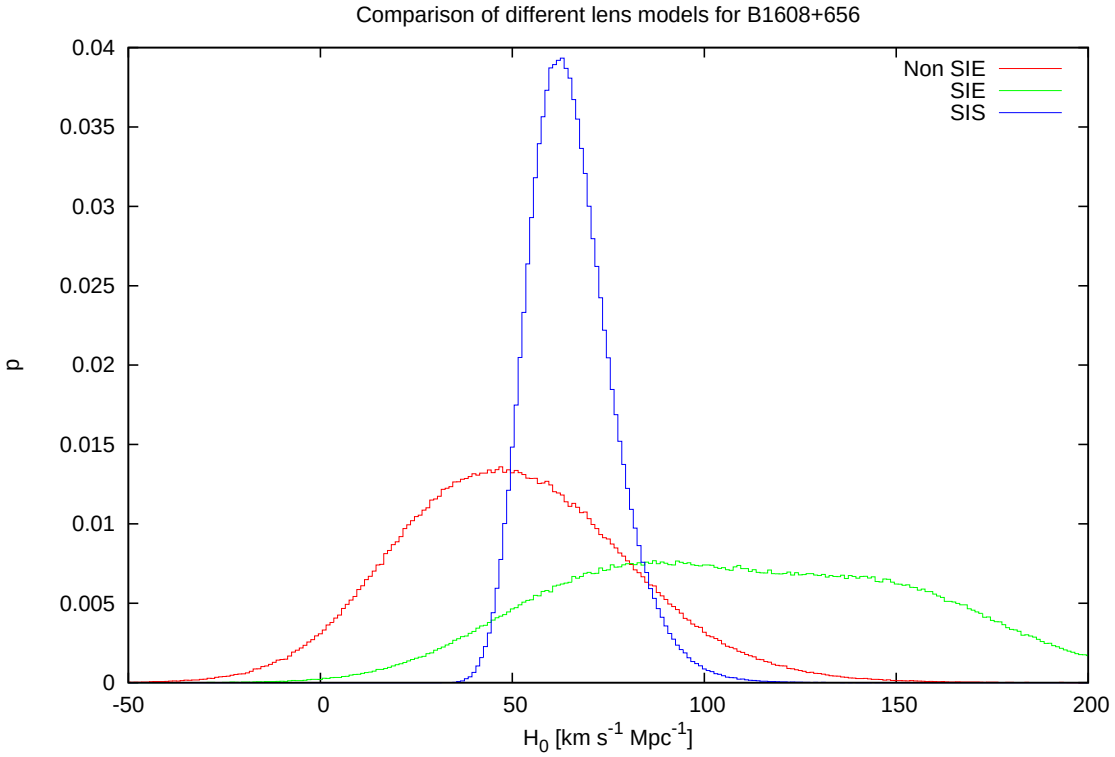

Figure 41: Comparison of a non singular isothermal ellipsoid and its simplifications. For each individual parameter we assume a Gaussian distribution with its associated errors and use a Monte Carlo simulation with 1 million calculations for each model.

lens model is more important than small error margins of single parameters. A more accurate measurement of the observable quantities will clearly constrain the error of Hubble's parameter but as Keeton and Kochanek already mentioned, we need a more complex model in order to gain better estimations.

If we however trust in the lens model proposed by Myers et al. we can present our estimation for the Hubble constant

$$H_0 = (48.3 \pm 26.7)\frac{\text{km}}{\text{s Mpc}} \tag{5.20}$$

which agrees with most other measurements presented in the section 2.3. We have to admit that this determination is based on model parameters provided by Myers et al. and that the method becomes evidently more complex if we have to estimate these values on our own. Nevertheless, this method enabled us to analyse the influence of the individual parameters, the dependence on the mass model and finally we obtained a probability distribution which yields the value of Hubble's parameter. Furthermore we were able to constrain the error margins of Hubble's parameter and we investigated that the errors of certain quantities and the lens model have to be improved in order to obtain more accurate estimations for Hubble's parameter.

References

[1] Plato. *Plato's cosmology: the Timaeus of Plato / translated with a running commentary by Francis MacDonald Cornford*. Routledge and Kegan Paul, London, 1937.

[2] A. Einstein. Kosmologische Betrachtungen zur allgemeinen Relativitätstheorie. *Sitzungsberichte der Königlich Preußischen Akademie der Wissenschaften (Berlin)*, pages 142–152, 1917.

[3] E. Hubble. A Relation Between Distance And Radial Velocity Among Extra-Galactic Nebulae. *Proceedings of the National Academy of Sciences*, 15, 1929.

[4] A. Sandage. Current problems in the extragalactic distance scale. *Astrophysical Journal*, 127:513–526, 1929.

[5] E. Komatsu et al. Five-Year Wilkinson Microwave Anisotropy Probe (WMAP) Observations: Cosmological Interpretation. *Astrophysical Journal*, 180:330–376, 2008.

[6] J. Huchra. Estimates of the Hubble Constant as part of the NASA/HST Key Project, 2010.

[7] H. T. Stokes. Computer resources for physics. Open Source, 2005.

[8] W. L. Freedman et al. The Hubble Constant. *Annual Review of Astronomy and Astrophysics*, 2010.

[9] A. G. Riess et al. Cepheid Calibrations of Modern Type Ia Supernovae: Implications for the Hubble Constant. *The Astrophysical Journal Supplement*, 183:109–141, July 2009.

[10] D. N. Spergel et al. First-Year Wilkinson Microwave Anisotropy Probe (WMAP) Observations: Determination of Cosmological Parameters. *The Astrophysical Journal Supplement*, 148:175–194, September 2003.

[11] E. Komatsu et al. Five-Year Wilkinson Microwave Anisotropy Probe Observations: Likelihoods and Parameters from the WMAP Data. *The Astrophysical Journal Supplement*, 180:306–329, February 2009.

[12] S. H. Suyu et al. Dissecting the Gravitational lens B1608+656. II. Precision Measurements of the Hubble Constant, Spatial Curvature, and the Dark Energy Equation of State. *Astrophysical Journal*, 711:201–221, March 2010.

[13] M. Bartelmann. Topical Review Gravitational Lensing. *Classical and Quantum Gravity*, 27(23):233001–+, December 2010.

[14] P. Schneider. *Extragalactic Astronomy and Cosmology*. 2006.

[15] R. Narayan and M. Bartelmann. Lectures on Gravitational Lensing. *ArXiv Astrophysics e-prints*, June 2008.

[16] P. Schneider, C. S. Kochanek, and J. Wambsganss. *Gravitational Lensing: Strong, Weak and Micro*. 2006.

[17] M. Bartelmann. General Relativity. Lecture Script, 2010.

[18] Time Travel Research Center. http://www.zamandayolculuk.com/.

[19] A. S. Eddington, C. Davidson and F.W. Dyson. A Determination of the Deflection of Light by the Sun's Gravitational Field, from Observations Made at the Total Eclipse of May 29, 1919. *Royal Society of London Philosophical Transactions Series A*, 220:291–333, 1920.

[20] O. Chwolson. Über eine mögliche Form fiktiver Doppelsterne. *Astronomische Nachrichten*, 221:329–+, June 1924.

[21] A. Einstein. Lens-Like Action of a Star by the Deviation of Light in the Gravitational Field. *Science*, 84:506–507, December 1936.

[22] R. F. Carswell, R. J. Weymann and D. Walsh. 0957 + 561 A, B: twin quasistellar objects or gravitational lens? *Nature*, 279:381–384, 1979.

[23] S. Refsdal. On the possibility of determining Hubble's parameter and the masses of galaxies from the gravitational lens effect. *Monthly Notices of the Royal Astronomical Society*, 128:307–+, 1964.

[24] NASA, ESA and STScI. Einstein Cross, 1990.

[25] NASA, ESA, A. Bolton (Harvard-Smithsonian CfA) and the SLACS Team. Einstein Ring, 2005.

[26] P. Schneider, J. Ehlers, and E. E. Falco. *Gravitational Lenses*. 1999.

[27] I. I. Shapiro. Fourth Test of General Relativity. *Physical Review Letters*, 13:789–791, December 1964.

[28] E. E. Falco, M. V. Gorenstein and I. I. Shapiro. On model-dependent bounds on H0 from gravitational images: Application to Q0957+561A,B. *Astrophysical Journal*, 289, 1984.

[29] C. S. Kochanek. What Do Gravitational Lens Time Delays Measure? *Astrophysical Journal*, 578:25–32, October 2002.

[30] C. S. Kochanek. Gravitational Lens Time Delays in Cold Dark Matter. *Astrophysical Journal*, 583:49–57, January 2003.

[31] M. Bartelmann. Arcs from a universal dark-matter halo profile. *Astronomy and Astrophysics*, 313:697–702, September 1996.

[32] P. Saha et al. The Hubble Time Inferred from 10 Time Delay Lenses. *Astrophysical Journal*, 650:L17–L20, October 2006.

[33] M. Oguri. Gravitational Lens Time Delays: A Statistical Assessment of Lens Model Dependences and Implications for the Global Hubble Constant. *Astrophysical Journal*, 660:1–15, May 2007.

[34] H. J. Witt, S. Mao and C. R. Keeton. Analytic Time Delays and H0 Estimates for Gravitational Lenses. *Astrophysical Journal*, 544:98–103, November 2000.

[35] NASA/STScI, ESA, S. H. Suyu and P. J. Marshall. Quadruple Lens System B1608-656 observed with the Advanced Camera for Surveys on HST.

[36] *C. R. Keeton and C. S. Kochanek. Ellipsoidal models for four-image lenses: implications for halactic structure and H0*, Harvard-Smihtsonian Center for Astrophysics, 1997.

[37] S. T. Myers et al. 1608+656: A Quadruple-Lens System Found in the CLASS Gravitational Lens Survey. *Astrophysical Journal*, 447:L5+, July 1995.

[38] L. V. E. Koopmans and C. D. Fassnacht. A Determination of H0 with the CLASS Gravitational Lens B1608+656. II. Mass Models and the Hubble Constant from Lensing. *Astrophysical Journal*, 527:513–524, December 1999.

Declaration

I declare that I have completed this thesis independently and that I have not used other than the declared sources. Sections that reflect the thoughts or works of others are made known through the definition of sources.
Heidelberg, 11.07.2011